3-2022

Estimating Atmospheric Turbulence Within a Short Exposure Frame Selection Algorithm

Aaron J. DeLuca

Estimating Atmospheric Turbulence Within a Short Exposure Frame Selection Algorithm

THESIS

Aaron J. DeLuca, 1st Lt, USAF

AFIT-ENG-MS-22-M-022

DEPARTMENT OF THE AIR FORCE
AIR UNIVERSITY

AIR FORCE INSTITUTE OF TECHNOLOGY

Wright-Patterson Air Force Base, Ohio

DISTRIBUTION STATEMENT A.
APPROVED FOR PUBLIC RELEASE; DISTRIBUTION UNLIMITED.

AFIT-ENG-MS-22-M-022

ESTIMATING ATMOSPHERIC TURBULENCE WITHIN A SHORT EXPOSURE FRAME SELECTION ALGORITHM

THESIS

Presented to the Faculty

Department of Electrical and Computer Engineering

Graduate School of Engineering and Management

Air Force Institute of Technology

Air University

Air Education and Training Command

In Partial Fulfillment of the Requirements for the

Degree of Master of Science in Electrical Engineering

Aaron J. DeLuca, BSEE

1st Lt, USAF

March 2022

AFIT-ENG-MS-22-M-022

ESTIMATING ATMOSPHERIC TURBULENCE WITHIN A SHORT EXPOSURE FRAME SELECTION ALGORITHM

Aaron J. DeLuca, BSEE

1st Lt, USAF

Committee Membership:

Maj David Becker, PhD
Chair

Dr. Stephen Cain, PhD
Member

Dr. Robert Mills, PhD
Member

AFIT-ENG-MS-22-M-022

Abstract

Space is becoming an increasingly crowded domain. As it becomes more congested, the ability to accurately detect and track objects, both natural and man-made, becomes more and more important. Having an accurate space surveillance network allows us to protect our own space assets while also maintaining awareness of foreign space assets and threats to our satellites such as debris and small meteorites. This means that the ability to detect small, dim objects is key to being able to protect our space assets. This thesis will seek to expand on and improve certain existing space object detection techniques and algorithms.

The objective of this thesis is to combine two space object detection techniques: atmospheric turbulence estimation and short exposure frame selection, to see if it is possible to produce an optimal or nearly optimal detection result with less information being given to the algorithm. Traditionally, space object detection algorithms require knowledge of the atmosphere in the location they are imaging, but the algorithm being introduced in this research seeks to estimate the atmospheric turbulence within the detection algorithm, without any prior knowledge of it. This will allow it to image areas where there is no accurate atmospheric modeling available. What was observed during the course of the research is that adding this atmospheric turbulence estimation actually improved detector performance, which was something that was initially unexpected.

Acknowledgements

I would like to thank my advisor, Major Becker, for his guidance, support, and assistance throughout this process. Your insight was invaluable to me throughout this process.

I would also like to thank my fiancé for her support and encouragement throughout my time at AFIT. I couldn't have done it without you.

Aaron J. DeLuca

Table of Contents

Page

List of Figures

Page

List of Tables

Page

ESTIMATING ATMOSPHERIC TURBULENCE WITHIN A SHORT EXPOSURE FRAME SELECTION ALGORITHM

1. Introduction

1.1 Motivation

The ability to detect and track space objects is critical to accomplishing our military and national security objectives. In the words of General John Raymond, the United States Space Force (USSF) Chief of Space Operations, "Space really underpins…all of our instruments of national power. It provides huge economic opportunity, scientific opportunity and military opportunity" [1]. Therefore, we must be able to protect our space objects from both unintentional collisions with space debris and from deliberate attacks by adversaries.

According to the National Aeronautics and Space Administration (NASA), there are currently over 27,000 pieces of space debris, both natural and man-made, being tracked by the Department of Defense's (DoD) Space Surveillance Network (SSN) sensors [2], and this number will only increase in the near future as more satellites are launched. In fact, according to NASA, even if all space launches stopped, the number of space debris objects would continue to increase due to collisions between existing space objects [3]. This ever-increasing amount of near-Earth orbit (NEO) objects means that the importance of detecting and tracking debris to avoid collisions with our space assets is increasingly important. Even a collision with a small piece of debris can cause catastrophic damage to a satellite due to the extreme speeds that space objects are traveling at (up to 17,500 miles per hour).

Another growing threat to our satellites is adversary action to deliberately degrade or destroy our space assets. According to Joint Publication 3-14, *Space Operations*, "Man-made threats can be physical or electromagnetic. They are further classified as intentional or unintentional, and it is vital to be able to differentiate between the two." [4]. This means that we need to be able to both detect satellites that are threats to our space assets and distinguish whether or not there was intentional action taken against our satellites. The combination of intentional and unintentional threats to our satellites from a combination of natural and man-made space objects poses an extraordinary challenge to our SSN, and means that improving our existing detection capabilities is critical is we are to keep pace with the ever-growing number of space objects.

1.2 Goals and Methods

The main goal of this research is to improve upon the existing matched filter and short exposure frame selection detection algorithms by enabling them to operate on short exposure data when they do not have prior knowledge of the atmospheric conditions where they are imaging. This research seeks to prove that both algorithms can provide similar levels of performance when estimating atmospheric turbulence as they can when they have pre-existing knowledge of the atmospheric turbulence where they are imaging. If successful, this research will allow both algorithms to maintain their detection performance while operating with less information

This research will be performed through simulation in MATLAB. The algorithms will be given simulated data sets to analyze, designed to replicate real-world conditions. These data sets will encompass a wide range of conditions such as imaging during

different times of day, imaging bright and dim objects, and having varying levels of background noise and atmospheric turbulence. Their detection performance will then be plotted on a Receiver Operating Characteristic (ROC) curve to determine the effectiveness of the modified algorithms. If successful, the ROC curves will show little to no drop off in detection performance when the algorithms estimate atmospheric turbulence versus when they have prior knowledge of the atmospheric turbulence at their imaging location.

1.3 Paper Outline

This thesis is divided into 5 chapters. In the introduction chapter, the importance of and need for this research is outlined. In chapter 2, literature review, background information on the detection algorithms used in this research, as well as noise, atmospheric turbulence, optical models, and data visualization are all introduced. Chapter 3 discusses the matched filter algorithm that was used for this research. It talks about how the matched filter is able to process short exposure data, how the simulated data that the algorithm processes was generated, and discusses the performance of both the detection algorithm and the Fried's seeing parameter (r_0) estimation accuracy. In chapter 4, the short exposure frame selection algorithm is introduced and the way is processes short exposure data is explained. This chapter also covers how the simulated short exposure data is generated and the algorithm performance both with and without r_0 estimation. Finally, the Conclusion chapter recaps the results that were found in chapters 3 and 4 and discusses whether or not the research goals introduced in chapter 1 were met. It also

highlights the importance of this research and its findings, identifies limitations of this research, and highlights opportunities for future work.

2. Literature Review

2.1 Chapter Overview

This chapter introduces some of the key factors and challenges that affect space object imaging and detection, as well as the current detection algorithms and methodologies that are currently used in the field. It will cover the different types of noise that can be found in images of space objects and how they are modeled in the simulation. r_0 is also introduced in this section as a method of estimating atmospheric turbulence so we can factor it into our detection algorithm. The concept of long and short exposure point spread functions (PSF)s are explained as a way to visualize the effects of atmospheric turbulence on images and the detection algorithm. This section also covers the different detection techniques that are used in this project as well as ROC curves, which are used to visualize the results.

2.2 Noise

One of the challenges in detecting objects in space, especially dim ones, is noise. Noise can have many causes, but the three we will look at in this research are background noise, photon counting noise, also known as shot noise, and readout noise. These three sources are the most common sources of noise in space object imaging, and therefore need to be included in the code to provide an accurate simulated dataset for the detection algorithms to process. In the case of long exposure imaging, readout noise is generally insignificant, however, for short exposure imaging, especially nighttime short exposure imaging, it tends to be a more significant source of noise, so a description of it is included in this section.

2.2.1 Background Noise

Background noise is any light coming from objects other than the one we are trying to detect. This can be from satellites, planets, stars, or any other objects capable of generating or reflecting light. Often background noise can be brighter than the object we are trying to detect, which presents a challenge to the detector in trying to pick out the dim object against a brighter background. In this research, the background value was estimated by taking the median value of the data over the whole image, as shown in Equation 1, where B is the background estimate, and $d(x, y)$ is the given image data over all the pixels in the image.

$$B = median\big(d(x, y)\big) \tag{1}$$

2.2.2 Photon Counting Noise

The other source of noise in this research is photon counting noise. This is noise that is caused by statistical quantum fluctuations in the number of photons arriving at the detector during a certain interval [5]. Even if the light source we are viewing is emitting a constant number of photons, those photons are independent of one another and therefore they do not arrive at the camera in a constant manner. The fluctuations in the number of photons being detected by the camera over time causes this photon counting noise. This kind of noise can be modeled by a Poisson distribution, which is what has been done in this research [5]. Equation 2 shows the equation for the probability mass function (PMF) of a Poisson random variable, where μ is the mean of the distribution and k is the number of occurrences.

$$P(X = k) = \frac{\mu^k e^{-\mu}}{k!} \tag{2}$$

2.2.3 Readout Noise

When a camera takes an image, the incoming photons are converted into electrons by the CCD array. They are then sent to an analog to digital converter which converts them into a digital signal. This analog to digital transformation can introduce a type of noise into the system known as readout noise. In many cases, this noise is insignificant, for example: in the long exposure case, the variance of the Gaussian distributed readout noise is much less than the variance of the photon counting noise, making the readout noise negligible. Also, in the daytime short exposure case, the higher photon counts in the images render the readout noise insignificant. In the nighttime short exposure case however, the readout noise can be significant enough that it can have a negative effect on the SNR of the image, especially if the image consists of several short exposure frames being averaged together, as in the case of our short exposure matched filter algorithm. This is because averaging frames together significantly increases the variance of the readout noise [6]. The equation for this variance is shown in Equation 3, where the variance of a given pixel in the image, $var\{d(x,y)\}$, is related to $\overline{K}$, which is the Poisson rate parameter, F, which is the number of frames being averaged together, and σ_{rn}^2, which is the variance of the readout noise.

$$var\{d(x,y)\} = F\overline{K} + F\sigma_{rn}^2 \tag{3}$$

2.3 Atmospheric Turbulence

Another obstacle to imaging space objects is atmospheric turbulence, which is what we seek to measure within our detection algorithms in this research. As light passes through the atmosphere, the atmosphere causes random phase delays that affect the detected image. These delays are caused by random fluctuations in the index of refraction of the air between the camera and the target [7]. The effect of these fluctuations on the detected image can cause it to look blurry, off-center, or have a number of other aberrations, which will be covered in the next section. Being able to understand and model the effect of the atmosphere on the image is critical to achieving optimal or near optimal matched filter and frame selector performance.

2.3.1 Zernike Polynomials

All optical systems have error. This error can be caused by many kinds of aberrations within the system, as well as external sources, such as atmospheric turbulence. One way to model the error introduced by these aberrations is with Zernike Polynomials. There are many different types of Zernike Polynomials, and they all describe the phase error introduced into an optical system by a certain type of aberration. The equation that describes the phase changes which capture the effect of all the aberrations present in an optical system is shown in Equation 4. In this equation, i is the index of the Zernike, $\Theta(u,v)$ is the equation describing the phase changes caused by the aberrations, C_i is the coefficient associated with the i^{th} Zernike, and $Z_i(u,v)$ is the i^{th} Zernike polynomial. The $\Theta(u,v)$ term will be used later in the chapter in the calculation

of the pupil function, which is used to calculate the optical transfer function (OTF) of our system.

$$\Theta(u,v) = \sum_i C_i Z_i(u,v) \tag{4}$$

In the case of this research, 84 Zernike Polynomials will be used, all of which describe a different type of error that can affect the image. Examples of errors that can be described by Zernike Polynomials are a loss of focus in the image, a tilt in the x or y direction, different astigmatisms within the image, and many more. Figure 1 shows an example of the first 15 Zernike polynomials, along with their names, which explain the effect they have on an image. For the purposes of this research, Zernike Polynomials will primarily be used to simulate the effects that atmospheric turbulence has on the images. They will also be used to create the phase screens that are used in the generation of the short exposure image data. This process will be explained further in chapter 4.

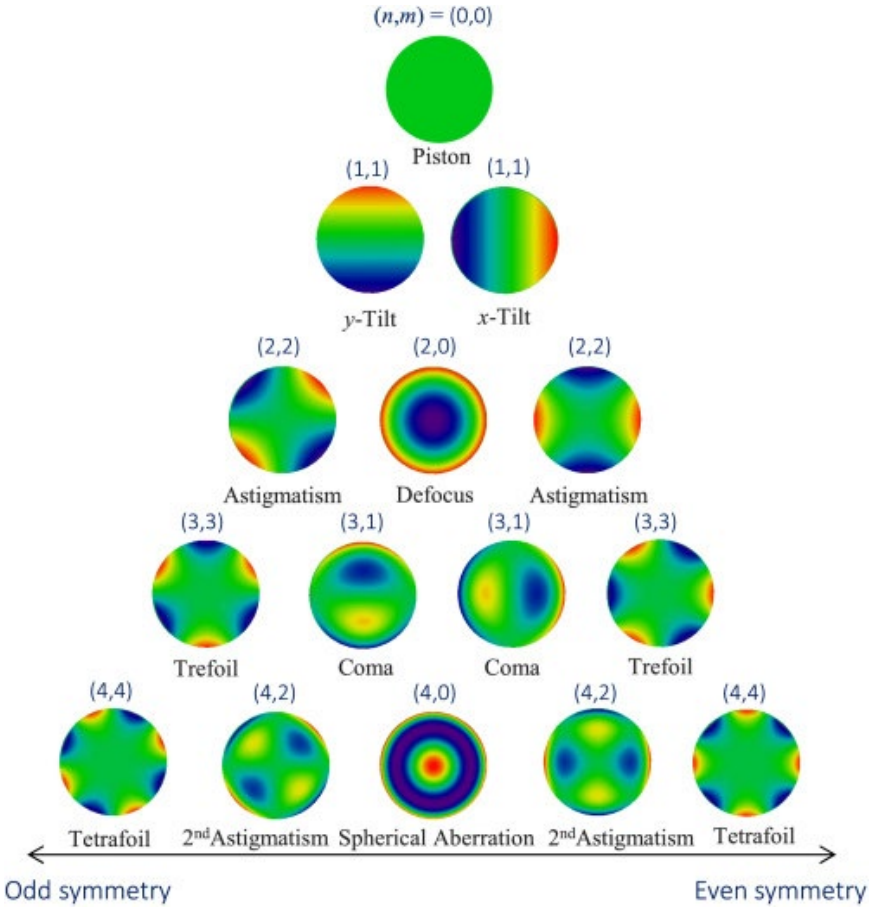

Figure 1: First 15 Zernike Polynomials

2.3.2 Fried's Seeing Parameter (r_0)

Fried's Seeing Parameter is a way to measure the turbulence at a given point in the atmosphere. It is measured in units of length, typically cm, and is defined as the diameter of a circular area over which the root mean square (RMS) wavefront error due to passage through the atmosphere is equal to 1 radian [8]. Any telescope with an aperture diameter greater than the r_0 value will have its resolution limited by the atmospheric turbulence unless it uses a method like adaptive optics to compensate for the effects of the atmosphere [9]. Real world r_0 values typically range from 2-10cm under

normal conditions but can be as good as 20cm or more under ideal conditions [8]. The equation for calculating r_0 is shown in Equation 5 below, where $\bar{\lambda}$ is the average wavelength of the light coming from the light source, C_n^2 is the strength of the atmospheric turbulence, and z is the distance between the light source and the aperture.

$$r_0 = 0.185\left(\frac{\bar{\lambda}^2}{zC_n^2}\right)^{\frac{3}{5}} \tag{5}$$

2.3.3 Long Exposure PSF

One of the ways to represent the atmospheric turbulence mentioned in the section 2.3 is through a long exposure PSF. Long exposure means that the camera shutter is left open for an extended period of time, allowing the detector to absorb more light, resulting in a more saturated image. A general rule is that images where the shutter is left open for substantially longer than 10ms are considered long exposure [5]. Example long exposure PSFs at different r_0 values are shown in Figure 2. By taking a long exposure image, the tilt caused by atmospheric turbulence can be averaged out over time, allowing us to get a more stable image than we would with shorted integration times. This allows us to understand the impact the atmosphere has on the data at each point in our image. Atmospheric modeling is critical to the performance of the matched filter, as it requires knowledge of the expected PSF from both the optics and the atmosphere. OTFs and PSFs are Fourier transform pairs, meaning that one is the Fourier transform of the other and vice versa. This means that if we know the PSF of a system we can calculate the OTF and vice versa. This is shown in Equations 6 and 7, where $H(f_x, f_y)$ is the OTF of our system and $h(x, y)$ is the PSF.

$$H(f_x, f_y) = \mathcal{F}(h(x,y)) \tag{6}$$

$$h(x,y) = \mathcal{F}^{-1}\left(H(f_x, f_y)\right) \tag{7}$$

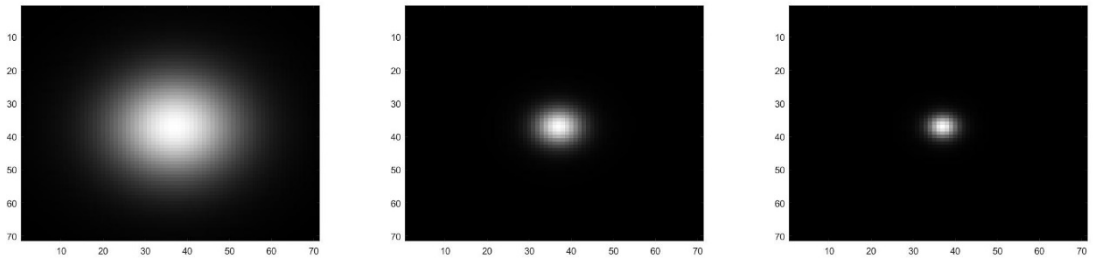

r_0=1cm r_0=3cm r_0=5cm

Figure 2: Example Long Exposure PSFs at Various r_0 Values

2.3.4 Long Exposure Optical Transfer Function (OTF)

To calculate our expected PSF, we need to know the OTF due to both our optics and the atmosphere. Assuming we know the properties of our telescope, we can calculate the OTF of the system due to the optics by taking the autocorrelation of the pupil function as shown in Equation 8, where $H_{opt}(f_x, f_y)$ is the OTF due to the optics, $P(x,y)$ is the pupil function of the optics, $P^*(x,y)$ is the conjugate of the pupil function, and $P^*(x - \lambda z f_x, y - \lambda z f_y)$ is the shifted conjugate of the pupil function. The equation for the pupil function is shown in Equation 9, where (u,v) are spatial locations, $\Theta(u,v)$ describes the phase changes that happen as a result of aberrations in the optical system, and $A(u,v)$ is the aperture function, which describes the opening in the optical system where the light enters.

$$H_{opt}(f_x, f_y) = \frac{\iint_{-\infty}^{\infty} P^*\left(x - \lambda z f_x, y - \lambda z f_y\right) P(x,y)\,dx\,dy}{\iint_{-\infty}^{\infty} P^*(x,y)P(x,y)\,dx\,dy} \tag{8}$$

$$P(u,v) = A(u,v)e^{j\Theta(u,v)} \tag{9}$$

Now that we have calculated the OTF due to the optics, we still need to calculate the OTF due to the atmosphere in order to calculate our total OTF. Equation 10 shows the calculation for the OTF due to the atmosphere, where $H_{atm}(v)$ is the long exposure OTF, λ is the mean wavelength of the incoming light, z is the focal length of the telescope, (f_x, f_y) is the spatial radial frequency, and r_o is the atmospheric seeing parameter, which is what we are trying to estimate within our detection algorithm in this research [7].

$$H_{atm}(f_x, f_y) = e^{-3.44\left(\frac{\lambda z(f_x,f_y)}{r_o}\right)^{\frac{5}{3}}} \tag{10}$$

Once the atmospheric and optical transfer functions have been calculated, the total OTF can be calculated by convolving the two together, as shown in Equation 11. We can now calculate our PSF by simply taking the inverse Fourier Transform of our OTF, as shown in Equation 12.

$$H_{tot}(f_x, f_y) = H_{atm}(f_x, f_y)H_{opt}(f_x, f_y) \tag{11}$$

$$h(x,y) = \mathcal{F}^{-1}\left(H_{tot}(f_x, f_y)\right) \tag{12}$$

2.3.5 Short Exposure PSF

As the names suggest, the difference between a long exposure and short exposure PSF is the length of time that the camera shutter is left open for. Generally, a short exposure image is one where the shutter is left open for 10ms or less [5]. In this thesis, 10 short exposure images are taken in quick succession to be fed to the detection algorithm. Short exposure imagery is generally used in scenarios where taking a long exposure image is not practical, such as daytime imagery, where taking a long exposure image

would produce a completely light saturated photo. There are also downsides to short exposure imagery, with the main one being that the object can appear to move around within the image from frame to frame due to the short exposure atmospheric induced tilt. This is referred to as jitter within the image and happens because the limited integration time does not allow the tilt of the image to be averaged out. This movement within the image frame can make it hard to detect an object over multiple frames. Examples of short exposure PSFs at different r_0 values can be seen in Figure 3.

Even though short exposure imagery can help work around the issue of saturation, there are still other challenges that it presents. One of these challenges is the much higher level of background noise present in the image. Even with a less saturated image, the background will still be much brighter than an image taken at dawn or at night, causing us to have a much lower image SNR. This makes it harder to discern the object we are trying to detect from the background.

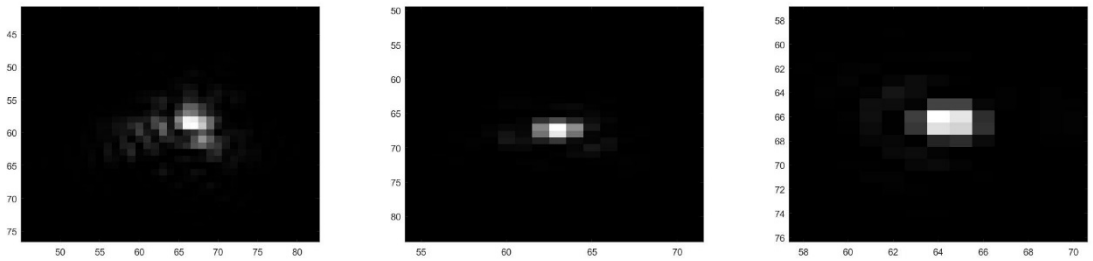

r_0=1cm r_0=3cm r_0=5cm

Figure 3: Short Exposure PSFs at Various r_0 Values

2.4 Image Model

Once we have calculated our PSF, we can calculate the total image formation model. Equation 13 is the general image formation model, where $h(x, y)$ is the PSF, γ is

the object brightness, and B is the background intensity. In this equation, gamma is a scaling factor because we assume that the object we are imaging is an unresolvable point source, and therefore gamma is just representing the brightness of said object. This equation was used to generate simulated images for testing the detection algorithm.

$$i(x, y) = \gamma h(x, y) + B \tag{13}$$

2.5 ROC Curves

The results of this project will be presented through ROC curves, which plot probability of detection (P_d) versus probability of false alarm (P_{fa}) over a full range of threshold values. Generating a ROC curve requires assuming that the statistics of the SNR values follow a Gaussian distribution [10]. Once this assumption is made, it allows us to generate a ROC curve based on the results of our 1000 trials. For this research, 1000 trials were chosen because that number provided a good middle ground between having enough trials to have an accurate sample dataset while not having too many to overload our available computing power. Without assuming a Gaussian distribution, it would take millions of trials to gather enough data to graph P_d and P_{fa} over the whole range of threshold values. This is because without the Gaussian assumption, you would have to run enough trials to have 50-100 false alarms at your chosen target false alarm rate, which for this project is 10^{-9}, meaning you would have to run about 10^{11} trials of your code. Since this is impractical, especially given the resources available for this research, the Gaussian assumption becomes a necessary aspect of generating the ROC curves. For the purposes of the frame selector portion of this research, a bi-modal Gaussian assumption is used, which will be explained further in chapter 4.

To generate a ROC curve, P_d and P_{fa} are first modeled as Gaussian distributions which allows them to be integrated over the range of threshold values. Equations 14 and 15 show how the P_d and P_{fa} values are calculated, where γ is the chosen threshold value, σ_{Λ_1} and σ_{Λ_0} are the standard deviation of the SNR values under h_1 and h_0, respectively, μ_{Λ_1} and μ_{Λ_0} are the mean of the SNR values under h_1 and h_0, respectively, and Λ is the variable being integrated over the range of threshold values.

$$Pd = \int_{\gamma}^{\infty} \frac{1}{\sqrt{2\pi}\sigma_{\Lambda_1}} e^{\frac{-(\Lambda-\mu_{\Lambda_1})^2}{2\sigma_{\Lambda_1}^2}} d\Lambda \tag{14}$$

$$Pfa = \int_{\gamma}^{\infty} \frac{1}{\sqrt{2\pi}\sigma_{\Lambda_0}} e^{\frac{-(\Lambda-\mu_{\Lambda_0})^2}{2\sigma_{\Lambda_0}^2}} d\Lambda \tag{15}$$

The results of this integration will be 2 sets of data that can be plotted against each other, with P_{fa} on the x axis and P_d on the y axis. This allows us to visualize the data as a curve and see what the P_d value will be for our desired P_{fa}.

2.6 Point Detector

One of the most basic and widely used space object detection algorithms is a point detector. A point detector is a simple way of detecting objects within a given pixel in an image. The specific point detector we will be looking at originated with the LINEAR program in 1995 as a way of advancing space object detection [11]. The Space Surveillance Telescope (SST) and several other space object detection assets still use a modified version of the LINEAR point detection algorithm [11]. It works by scanning each pixel in an image to determine the number of photons in that pixel. It then takes the

median value of all the pixels to determine an average background value. Finally, every pixel in the image is compared to the background value. Pixels that exceed the background value by a number of standard deviations equal to or greater than the threshold are determined to contain an object. The threshold value is set by the user to achieve a desired P_{fa}. This is done by modeling the likelihood ratio test (LRT) values as Gaussian distributions and then integrating them from a chosen threshold to infinity. The result of the integrals will be the P_d and P_{fa} for the chosen threshold value. Higher threshold values decrease the P_{fa}, but also decrease the P_d while the inverse is true for lower threshold values.

To derive the equation for the signal-to-noise ratio (SNR) for the point detector, we first must start out with a LRT, as shown in Equation 16. This is a simple way of testing two hypotheses to determine which one is more likely under certain conditions. For this example, our LRT is a ratio of the joint conditional probability density functions (PDF)s of the data. In this case, Λ is our LRT, d is the data collected from our sensor, h_1 is the condition that there is an object present, and h_0 is the condition that there is no object present. If $\Lambda>1$, our LRT says that there is an object present, and if $\Lambda<1$, we assume there is no object present.

$$\Lambda = \frac{P(d|h_1)}{P(d|h_0)} \underset{h0}{\overset{h1}{\gtrless}} 1 \tag{16}$$

The next step in deriving the SNR equation for the point detector is to assume a Gaussian model for the data. Once that is done, we can write equations for $P(d|h_0)$ and

$P(d|h_1)$, which are shown in Equations 17 and 18 below, where σ is the standard deviation of the data, s_{PD} is the signal from the object being looked at, and B is the background value. In both of these equations, the variance is assumed to be the same, meaning that the mean is the only thing that is changing due to the inclusion is the signal from the object we are detecting.

$$P(d|h_1) = \frac{1}{\sqrt{2\pi}\sigma} e^{\frac{-(d-s_{PD}-B)^2}{2\sigma^2}} \tag{17}$$

$$P(d|h_0) = \frac{1}{\sqrt{2\pi}\sigma} e^{\frac{-(d-B)^2}{2\sigma^2}} \tag{18}$$

We can now substitute Equations 17 and 18 into Equation 16, which, after some simplification, becomes Equation 19.

$$\Lambda = e^{\frac{2s_{PD}(d-B)-{s_{PD}}^2}{2\sigma^2}} \underset{h0}{\overset{h1}{\gtrless}} 1 \tag{19}$$

However, we do not want the LRT to be dependent on the signal coming from the object being looked at, so further simplification is required to remove s_{PD} from the equation. The first step to doing this is to take the natural log of both sides to remove the exponent, as shown in Equation 20.

$$ln(\Lambda) = \frac{2s_{PD}(d-B)-{s_{PD}}^2}{2\sigma^2} \underset{h0}{\overset{h1}{\gtrless}} 0 \tag{20}$$

We can then simplify and bring s_{PD} to the right side of the equation, resulting in Equation 21.

$$\frac{(d-B)}{\sigma} \underset{h0}{\overset{h1}{\gtrless}} \frac{s_{PD}}{2\sigma} \tag{21}$$

The final step is to substitute the right side of the equation for a threshold value, γ, which turns the LRT into the final form of the point detector SNR calculation, Equation 22,

$$SNR_{PD}(x,y) = \frac{(d(x,y) - B)}{\sigma} \underset{h0}{\overset{h1}{\gtrless}} \gamma \tag{22}$$

where (x,y) is the location of the pixel being examined, $d(x,y)$ is the value of the data at that pixel, B is the background radiation, which for this research is the median value of the data, σ is the standard deviation of the data, and γ is the user-chosen threshold value.

2.7 Matched Filter

One of the two detection algorithms that this research is centered on is the matched filter. While this algorithm is primarily used on long exposure data, it can also be used to process short exposure data, which is what is done in this research. The matched filter algorithm works by correlating the background subtracted data with the expected long exposure PSF. It then compares that value to the selected threshold to determine whether an object is present [12]. This algorithm requires knowledge of the expected PSF to achieve an optimal result, meaning it requires accurate atmospheric modeling of the area you are trying to image to provide a good model of the expected PSF. An inaccurate atmospheric model can cause a significant drop in the performance of the matched filter, which is shown in the results section.

To derive the equation for the SNR for the matched filter, we first must start out with a LRT, as shown in Equation 23. This is a simple way of testing two hypotheses to determine which hypothesis the data more closely resembles. In this case, Λ is our LRT, $d(x,y)$ is the data collected from the sensor, (x,y) are the coordinates of a given

pixel in the image, h_1 is the condition that there is an object present, and h_0 is the condition that there is no object present. Since the matched filter is looking at the entire image, instead of one pixel at a time like the point detector, it must encompass all the pixels in the image, which is why $\forall(x,y)$ is present in our LRT equation. If $\Lambda>1$, our LRT says that there is an object present, and if $\Lambda<1$, we assume there is no object present. In Equation 23, $P(d(x,y)|h_1)$ is the joint conditional PDF of the data when the object is present and $P(d(x,y)|h_0)$ is the joint conditional PDF of our data with no object present.

$$\Lambda = \frac{P(d(x,y)|h_1)\forall(x,y)}{P(d(x,y)|h_0)\forall(x,y)} \tag{23}$$

If we make the assumption that our data is Gaussian and the pixels in the image are independent, we can then use that Gaussian assumption to write the conditional PDFs for $P(d(x,y)|h_0)$ and $P(d(x,y)|h_1)$, which are shown in Equation 24 and 25 for the two hypotheses.

$$P(d(x,y)|h_1) = \prod_{x=1}^{N}\prod_{y=1}^{N}\frac{1}{\sqrt{2\pi}\sigma}e^{\frac{-(d(x,y)-S_{MF}h(x,y)-B)^2}{2\sigma^2}} \tag{24}$$

$$P(d(x,y)|h_0) = \prod_{x=1}^{N}\prod_{y=1}^{N}\frac{1}{\sqrt{2\pi}\sigma}e^{\frac{-(d(x,y)-B)^2}{2\sigma^2}} \tag{25}$$

where (x,y) is the location of the pixel being examined, $d(x,y)$ is the value of the data at that pixel, B is the background radiation, S_{MF} is the scaled irradiance from our target, σ is the standard deviation of the data, and $h(x,y)$ is the expected long exposure PSF. Plugging Equations 24 and 25 into Equation 23 and simplifying then gives us Equation 26.

$$\Lambda = \prod_{x=1}^{N}\prod_{y=1}^{N} e^{\frac{(d(x,y)-B)S_{MF}h(x,y)-{S_{MF}}^2h^2(x,y)}{2\sigma^2}} \underset{h0}{\overset{h1}{\gtrless}} 1 \tag{26}$$

To remove the exponential from the left side of Equation 26, we can take the natural log of Λ. Taking the natural log of a product converts it into a sum, which can be seen in Equation 27. Equation 27 shows the log-likelihood ratio test, which is the result of the described transformation.

$$L = \ln(\Lambda) = \sum_{x=1}^{N}\sum_{y=1}^{N} \frac{2(d(x,y)-B)S_{MF}h(x,y)-{S_{MF}}^2h^2(x,y)}{2\sigma^2} \underset{h0}{\overset{h1}{\gtrless}} 0 \tag{27}$$

We do not want our LRT to be dependent on the intensity of our target, S_{MF} , so further simplification to remove the dependency is required. Once S_{MF} has been removed from the left side of the equation, the right side can now be substituted for a user-defined threshold value, γ as shown in Equation 28.

$$L = \sum_{x=1}^{N}\sum_{y=1}^{N}(d(x,y)-B)h(x,y) \underset{h0}{\overset{h1}{\gtrless}} \sum_{x=1}^{N}\sum_{y=1}^{N}\frac{S_{MF}h(x,y)}{2} = \gamma \tag{28}$$

Equation 28 is still not the final form of the SNR calculation though, because the left side of the equation needs to be a zero mean, unit variance Gaussian random variable in order for us to be able to use γ to set our false alarm rate. Calculating the mean and variance of the left side gives us the completed form of the SNR equation, as shown in Equation 29.

$$SNR_{MF}(x,y) = \frac{\sum_{x=1}^{N}\sum_{y=1}^{N}h(x,y)(d(x,y)-B)}{\sigma_n\sqrt{\sum_{x=1}^{N}\sum_{y=1}^{N}h^2(x,y)}} \underset{h0}{\overset{h1}{\gtrless}} \gamma \tag{29}$$

2.8 Short Exposure Frame Selection

The other detection algorithm featured prominently in this research is the short exposure frame selector. Unlike the matched filter, this algorithm is designed exclusively for processing short exposure imagery, making it ideal for this research. In section 2.3.3, the use of a long exposure PSF to model the effects of atmospheric turbulence was explained. While a long exposure PSF is ideal for our detection algorithm, there are scenarios where one might not be available, and we need to rely on a series of short exposure images instead of one long exposure image for our detection algorithm. The problem with short exposure images is that due to the lessened exposure time, some of the frames may not be fully saturated and therefore may not fully capture an image of the object we are trying to detect. They also do not have the image tilt averaged out, meaning that there can be significant movement between frames. The combination of these two factors means that we need to find a way to only send the best frames to our detection algorithm. To accomplish this, we need to use a frame selection algorithm.

The frame selection algorithm being used in this research was originally introduced by Becker in his dissertation research and further improved by Paw in his research [6,13]. Instead of one long exposure image, the algorithm starts with 10 short exposure images, with each one having an integration time of 10-25ms. The algorithm starts by ranking the frames. It does this by convolving the summation of all the frames minus the background against the expected long exposure PSF to provide an average SNR value. It then removes one frame at a time and repeats the first step, calculating the average SNR with that frame missing. It then adds that frame back into the dataset and repeats the process for a different frame until it does this for every frame in the group.

Once each frame has an average SNR associated with its removal from the group, the algorithm is able to rank them. The frames that decreased the average SNR the most when they were removed are ranked as the best frames, and the frames that increased the average SNR the most upon their removal are ranked as the worst frames. The equation describing this process is shown below in Equation 30, where $SNR_{FS}(n)$ is the average SNR with the nth frame removed, $d_k(x,y)$ is the frame being looked at, $h(x,y)$ is the expected PSF, and B is the background radiation.

$$SNR_{FS}(n) = \sum_{k=1,k\neq n}^{n} (d_k(x,y) - B) * h(x,y) \tag{30}$$

Once the frames are sorted, then the removal process begins. The algorithm calculates the average SNR with all the frames in the group, then it removes the lowest ranked frame and recalculates the SNR value. It repeats this process until removing frames no longer increases the average SNR value by a significant amount. Once this is achieved, the remaining frames are the ones that get passed to the detection algorithm. Using this process ensures that only the best frames are used in the detection algorithm [13].

One key similarity between the SNR calculations for the matched filter and frame selector is that they both rely on $h(x,y)$, which is the expected PSF of the object being detected. One of the key pieces of data required to calculate the expected PSF is the r_0 value of the atmosphere where they are imaging. This is where r_0 estimation comes into play and why it is a key aspect of this research. We want to be able to determine the expected PSF without having prior knowledge of what the r_0 value is and introducing this sort of estimation into the short exposure case in the main novel aspect of this research.

2.9 r_0 Estimation

The critical aspect of this research that differentiates it from research done on similar topic areas in the past is the introduction of r_0 estimation into short exposure space object detection algorithms. As Equations 29 and 30 show, both the matched filter and frame selector SNR calculations are reliant on knowledge of the expected PSF to produce an optimal result. However, if we do not have an accurate atmospheric model of the area we are trying to image or want to check the accuracy of our model, having the detection algorithm estimate r_0 can be very useful. The r_0 estimation method that is used in this research was developed by former AFIT student Captain Grant Graupmann for his thesis [14] and has been adapted for use in the short exposure case for this research.

The r_0 estimation algorithm starts by generating 50 r_0 values over a range specified by the user. For this research, the range that was chosen was between 0-5cm. It then creates a PSF for each r_0 value, examples of which are shown in Figure 4, and correlates each PSF with the given frame of data for that trial. It then finds the r_0 value used to create the PSF produced the highest SNR when correlated with the image and uses that r_0 value as the estimated r_0 for that trial. It repeats this process for all 1000 trials, producing an independent r_0 estimate for each trial. Once all 1000 trials have been run, the 1000 estimated r_0 values are averaged together to provide an overall estimated r_0. The calculation for this estimation method is shown in Equation 31, where N is the number of trials and $r_{0_{max}}(x)$ is the r_0 value that produces the highest SNR for that given trial.

$$r_{0_{est\ total}} = \frac{\sum_{x=1}^{N=1000} r_{0_{max}}(x)}{N} \tag{31}$$

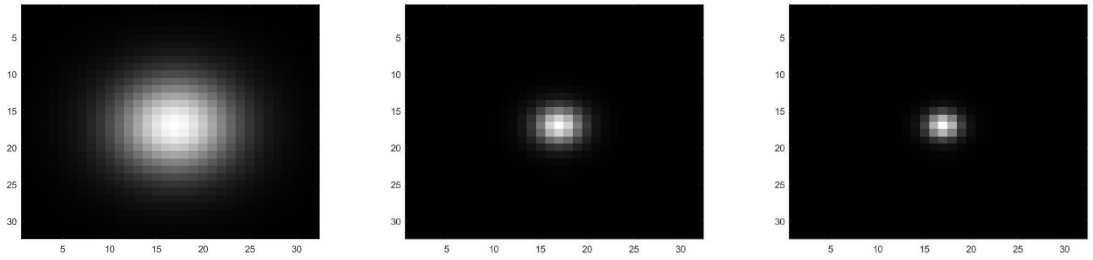

r_0=1cm r_0=3cm r_0=5cm

Figure 4: Generated PSFs at Different r_0 Values

3. Short Exposure Matched Filter Algorithm

3.1 Chapter Overview

The purpose of this chapter is to cover in detail the Matched Filter algorithm that was used in this research. While a basic definition of the matched filter was provided in chapter 2, it will be explored further in this chapter. The concept of using a matched filter on short exposure data will be introduced and explained in detail. One of the key aspects of this research is the ability of the detection algorithms to estimate atmospheric turbulence while having no knowledge of it beforehand, and the ability of the matched filter to do so will be discussed. Finally, the results of the matched filter algorithm used in this research will be shown and the performance of the algorithm will be analyzed.

3.2 Matched Filter With Long vs. Short Exposure Data

The matched filter is a space object detection algorithm that is most often used to process long exposure data. This is because a long exposure image does not have the limitations, mainly lack of image saturation and movement within the frame, that come with short exposure imagery. In addition, long exposure imagery is usually taken at night, where the background radiation in minimal and the object is easiest to distinguish from the background, which also improves detector performance. However, the focus of this research is optimizing detector performance using short exposure, daytime imagery. This means that the algorithm will have to be adapted to handle the challenges that come with processing short exposure image data.

3.3 Simulated Long Exposure Image

Unlike the Frame Selector algorithm that will be covered in the next chapter, the Matched Filter is not given the raw short exposure data to process. Running the matched filter algorithm on individual short exposure frames would result in poor detector performance and inaccurate results. To allow the matched filter to produce an accurate result using short exposure data, we instead sum up the 10 frames of short exposure data to create one composite image, which is our "simulated" long exposure image that is then fed into the algorithm. This helps to mitigate the adverse effects of the short exposure integration time by providing a brighter image of the object as well as averaging out the jitter in the image. An example simulated long exposure image can be seen in Figure 5, along with several of the short exposure frames that were combined together to generate it. This allows our matched filter to operate similarly to the way it would if it were being given an actual long exposure image.

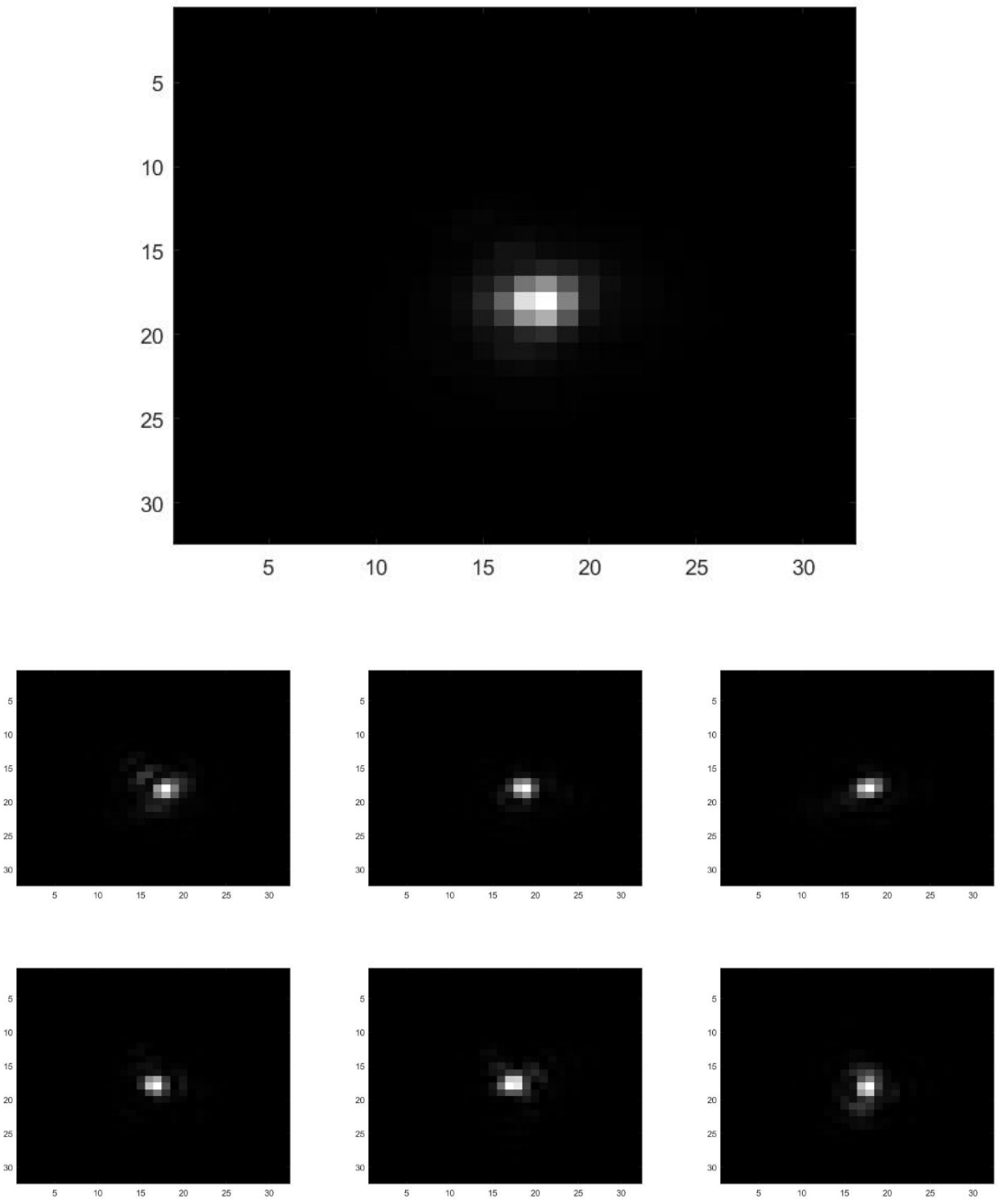

Figure 5: Simulated Long Exposure Image With no Noise and Six of the Ten Frames That Were Combined to Generate it

3.4 Simulated Data

The data used in this experiment was generated using varying sets of parameters to represent a wide range of simulated real-world conditions. The background radiation, object SNR, and true r_0 value were all varied over a range of values to represent imaging at different times of day, different object brightness levels, and different atmospheric turbulence conditions. Table 1 lists the different values of each parameter and what each one represents. These different simulated conditions will be referenced in the results section when evaluating detection performance.

Table 1: Simulated Data Parameters

Parameter	Value(s)
Background Radiation	1000 Photons (Daytime) 100 Photons (Dusk/Dawn) 10 Photons (Night)
Object SNR	0.75 (Dim Object) 1 (Normal Object) 1.5 (Bright Object)
r_0 Value	0-5 cm
Wavelength of Light	0.5 μm
Telescope Diameter	5.08 cm

3.5 Estimating r_0

The key aspect of this research is being able to estimate r_0 when we do not have any prior knowledge of it. In the code, the r_0 estimation is done before either of the detection algorithms is run in order to use that estimate in the algorithms. r_0 is estimated similarly to the methods described in section 2.8. First, 50 PSF's are generated using 50 different r_0 values ranging between 0-5cm. Then, each of those PSFs are correlated with

the simulated long exposure image for that given trial. The r_0 used to generate the PSF that matches the given frame of data most closely is then chosen as the estimated r_0 for that trial. This process is repeated for all 1000 trials, then at the end of the 1000 trials, all 1000 independent r_0 estimates are averaged together to provide a mean r_0 estimate, which should be close to the true r_0 for that run of the code.

3.6 Results

This section will cover the results of the short exposure matched filter research with r_0 estimation. The detector performance under different conditions will be plotted and analyzed. Each of the variables listed in Table 1 will be varied while the other variables are held constant in order to provide a visualization of how each one of them effects the results. Also, the r_0 estimation accuracy will be tested and the results on both a trial-by trial basis and an overall average will be covered.

3.6.1 r_0 Estimation Accuracy

In the long exposure case, the estimated r_0 is usually very close to the actual r_0, and the algorithm using the estimated r_0 performs slightly worse than the algorithm with the true r_0 due to the difference. In the short exposure case, the average estimated r_0 differs from the true r_0 much more on a trial-by-trial basis, although the average value over all 1000 trials still remains close to the actual value. Examples of this can be seen in Table 2, which shows trial-by-trial r_0 estimates to illustrate the fluctuations that occur in the estimation with each individual trial. It also shows the average SNRs over all 1000 trials in the final column. The reason for this variance is the short exposure data that is being used. Due to aberrations in the images, the actual r_0 value can change from frame to

frame, meaning the r_0 value of many of the images being used is not actually the true r_0 value of the atmosphere at that point. This means that the estimated r_0 is often more accurate for a given image than the true r_0 for many of the images being tested.

Table 2: r_0 Estimates

	Trial Number							
True r_0	**1**	**2**	**3**	**4**	**5**	**6**	**7**	**Total r_0 est (All 1000 trials)**
1cm	0.3cm	1.3cm	3.7cm	0.7cm	0.2cm	0.7cm	2.4cm	1.58cm
2cm	1.6cm	3.1cm	1.7cm	1.8cm	2.2cm	1.3cm	1.6cm	2.44cm
3cm	2.8cm	3.2cm	3.7cm	2.8cm	3.3cm	5.0cm	3.3cm	3.25cm
4cm	5.0cm	3.7cm	1.6cm	3.0cm	2.1cm	2.9cm	5.0cm	3.96cm
5cm	4.0cm	5.0cm	5.0cm	4.9cm	3.0cm	2.9cm	5.0cm	4.42cm

3.6.2 ROC Curves – Time of Day

In order to test the impact that r_0 estimation had on the matched filter algorithm, it was run twice on the same set of data. One of the runs used r_0 estimation in order to estimate r_0 for each trial, while during the other run the matched filter algorithm was given the true r_0 value. This allowed us to generate two ROC curves, one for the matched filter using r_0 estimation and one for the matched filter using the true r_0. This provides a fair performance comparison because both algorithms are analyzing the exact same data,

the only thing that changes is the method by which they get their r_0 value. We then held all of the other variables the same and only varied the time of day between dusk/dawn, day, and night in order to see what effect they had on the performance of the detector.

When looking at the ROC curves generated by the code, the matched filter using r_0 estimation outperforms the matched filter without r_0 estimation in every case we tested, as shown in Figures 6-8. In these trials, P_d increases by an average of 21% at the chosen P_{fa} value of 10^{-9}, which is a standard target P_{fa} value for space object detection applications. This is due to the factors listed in the previous section causing our estimated r_0 to be more accurate than the true r_0 for many of the images being processed. This performance increase is something that would never be seen in the long exposure case, due to the image r_0 always being almost exactly equal to the true r_0 in long exposure images. This provides a good illustration of the differences that using short exposure imagery can cause in a detection algorithm.

One trend shown in the figures that would seem to refute the idea that r_0 estimation causes an increase in performance is the fact that in all 3 ROC curves shown, the matched filter without r_0 estimation overtakes the one with r_0 estimation at a P_{fa} value of approximately 10^{-3}. The reason that we do not consider this to be significant is because a P_{fa} value that high represents too high a level of uncertainty for almost any space object detection application. As mentioned earlier, 10^{-9} is a standard P_{fa} value to choose to measure P_d at, and the one that is used to evaluate all ROC curves in this research. A P_{fa} value of 10^{-3} which is orders of magnitude larger would introduce too

many false alarms into the data, making it hard to trust the performance of the detection algorithm.

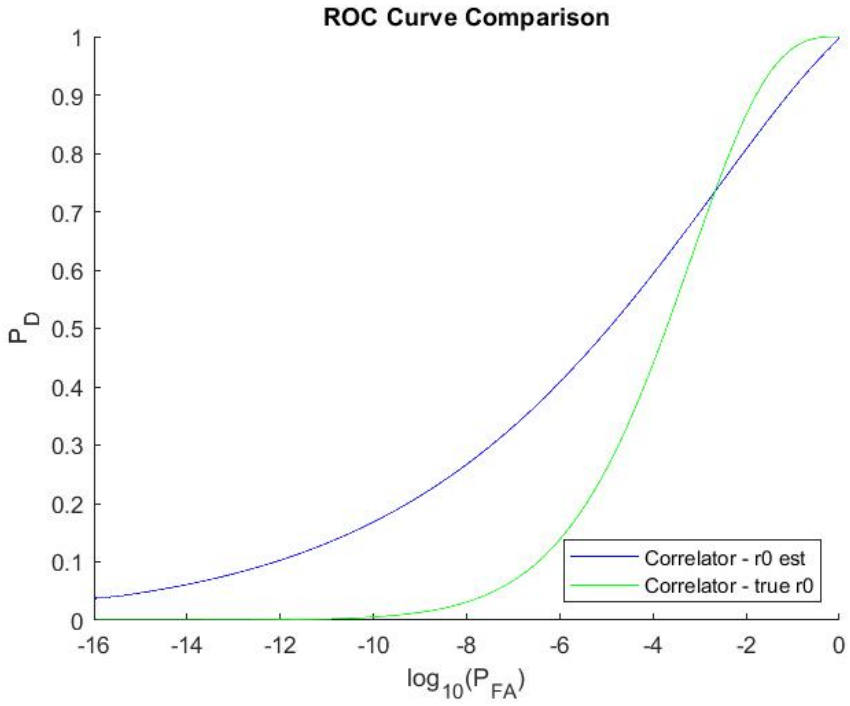

Figure 6: Matched Filter Performance (Dusk/Dawn Conditions, SNR=1, r_0=2.5cm)

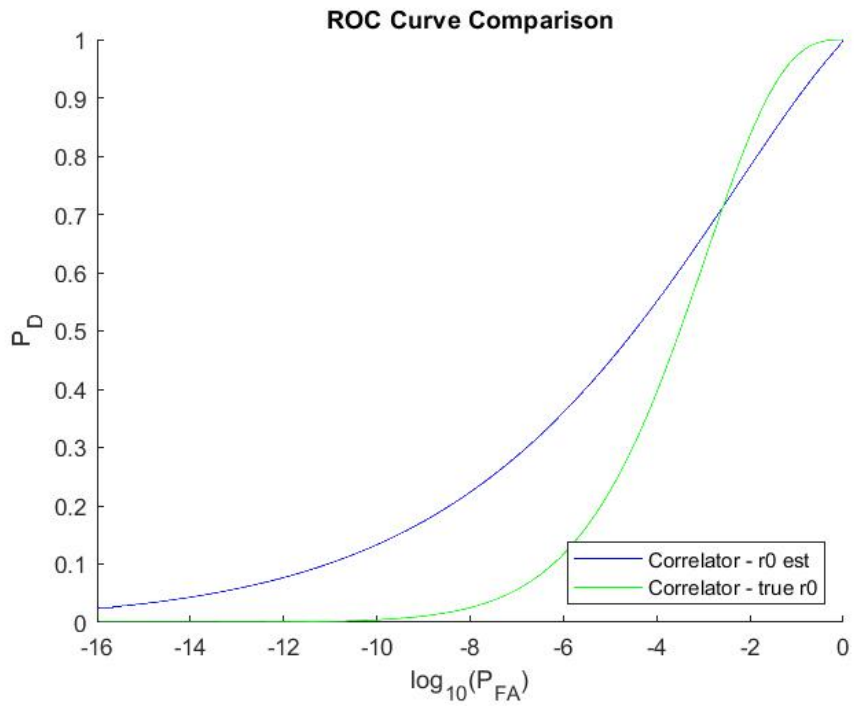

Figure 7: Matched Filter Performance (Day Conditions, SNR=1, r_0=2.5cm)

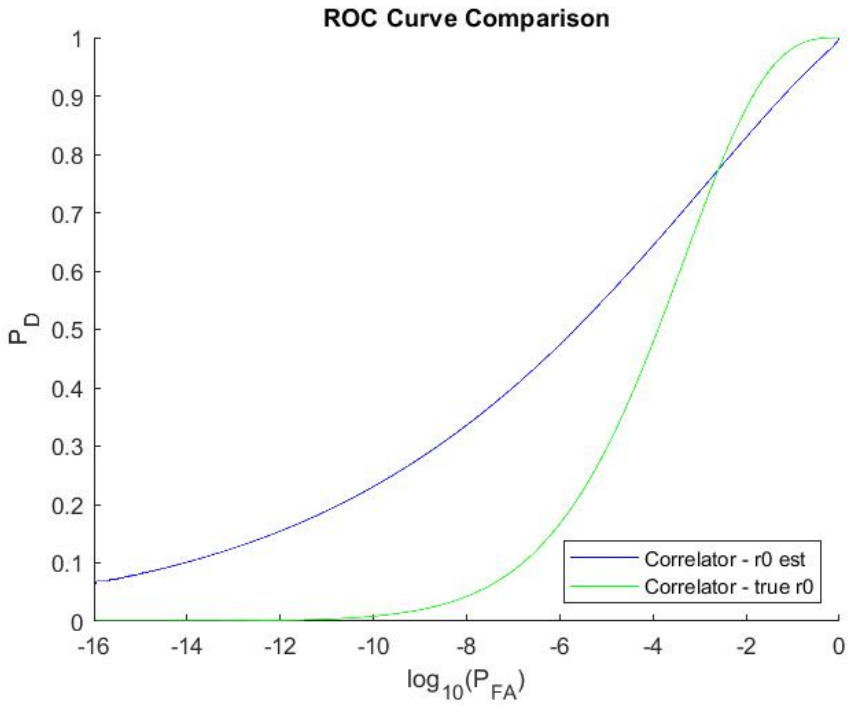

Figure 8: Matched Filter Performance (Night Conditions, SNR=1, r_0=2.5cm)

3.6.3 ROC Curves – Changes in True r_0

Similarly to the last section, this section will show 3 different ROC curves to compare the performance of the matched filter with and without r_0 estimation. This time however, the variable being changed will be the true r_0 value used to generate the simulated data. This allows us to see what effect the true r_0 has on our matched filter algorithm both with and without r_0 estimation. As shown in Figures 9-11, at an extremely low r_0 value such as 1cm, both detectors have a P_d of essentially 0% at our target P_{fa} value of 10^{-9}, but the matched filter without r_0 estimation does outperform slightly at higher P_{fa} values. As the true r_0 value increases, the performance of both detectors, measured in terms of P_d, increases as well, however, the performance of the matched filter with r_0 estimation increases more than the performance of the matched filter without r_0 estimation the higher the true r_0 goes. They are practically equal at a low r_0 of 1cm, then at 2.5cm the matched filter with r_0 estimation performs about 20% better than the one without at P_{fa}= 10^{-9}, and at an r_0 of 4 cm, that performance increase jumps to almost 50%.

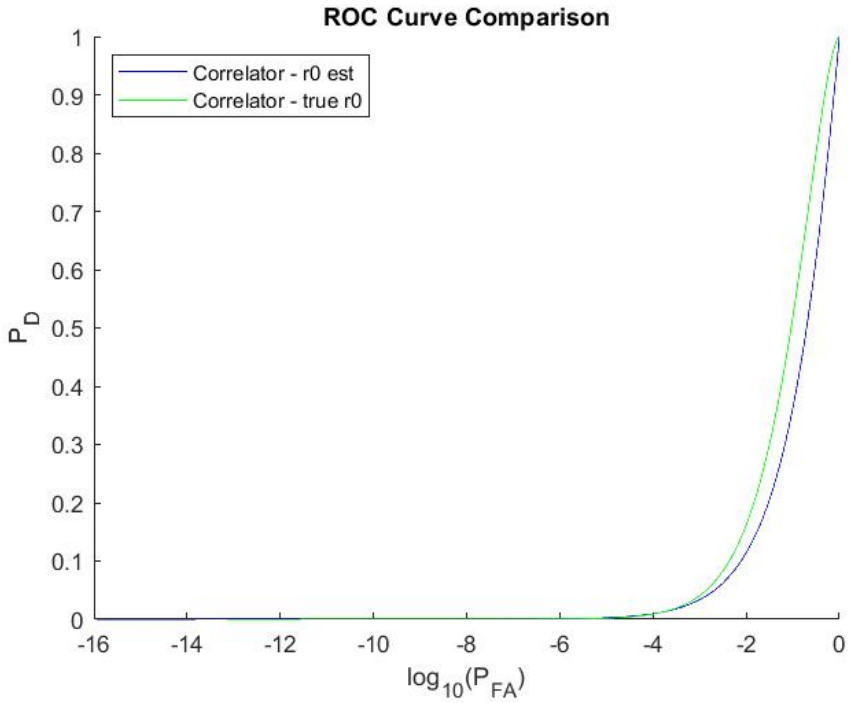

Figure 9: Matched Filter Performance (Day Conditions, SNR=1, r_0=1cm)

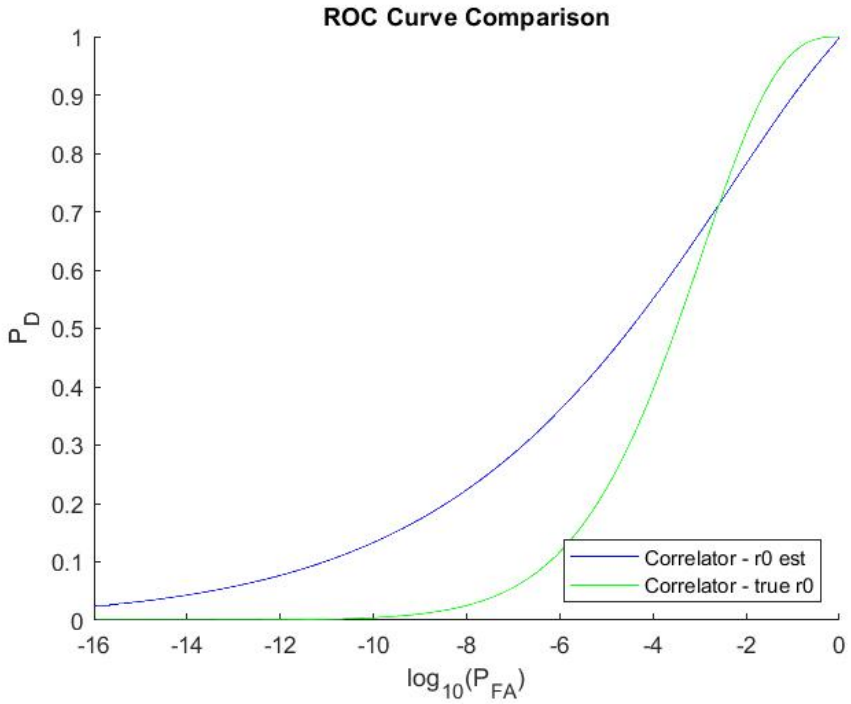

Figure 10: Matched Filter Performance (Day Conditions, SNR=1, r_0=2.5cm)

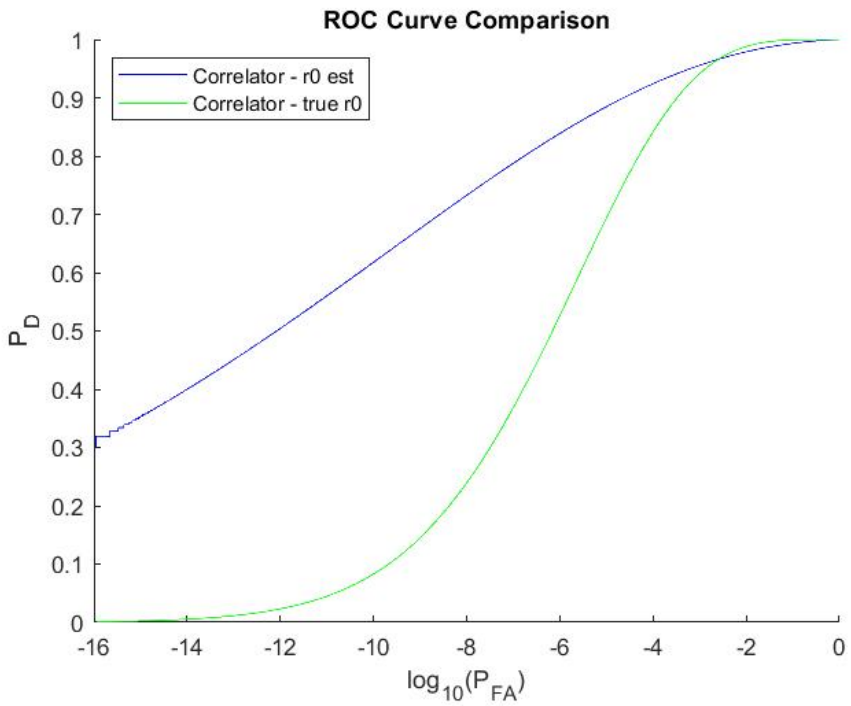

Figure 11: Matched Filter Performance (Day Conditions, SNR=1, r_0=4cm)

3.6.3 ROC Curves – Object Brightness

The final variable to be tested is the brightness of the object being imaged. As with the other variables being tested, 3 ROC curves will be generated, with the only difference between them being the brightness of the simulated image. Then the comparison of the matched filter with and without r_0 estimation will be shown in order to see what effect the object brightness has on our detection algorithms. Figures 12-14 show the results of this testing. As expected, a brighter object being imaged leads to better detector performance. Like the last section with the changes in the true r_0 value, the performance of the matched filter with r_0 estimation did increase by more than the matched filter without r_0 estimation, going from about an 8% increase at SNR=0.75 to

20% at SNR=1 to 29% at SNR=1.5. However, these performance gains are not as extreme as the changes due to the shift in true r_0 value.

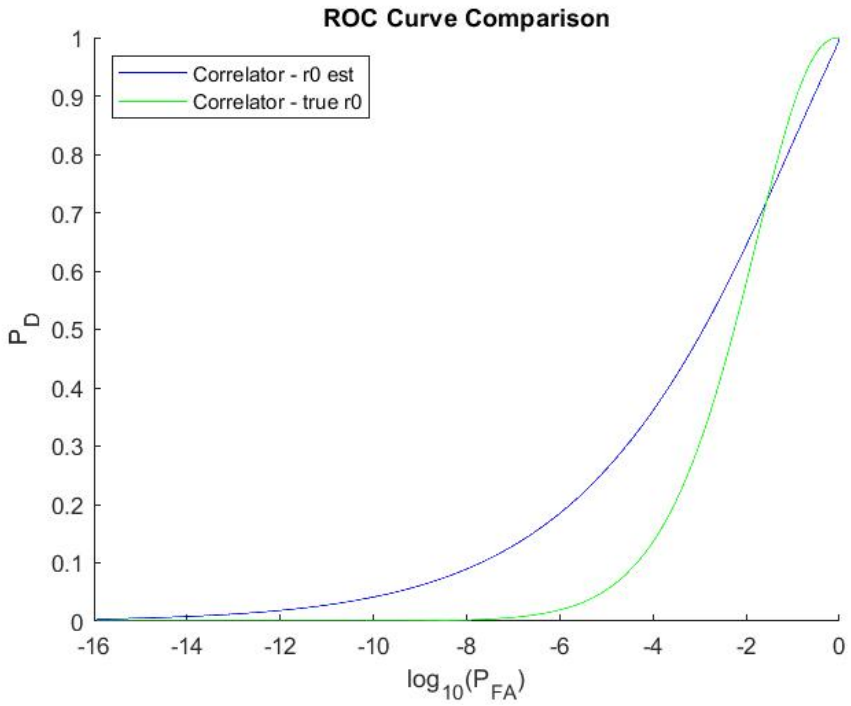

Figure 12: Matched Filter Performance (Day Conditions, SNR=0.75, r_0=2.5cm)

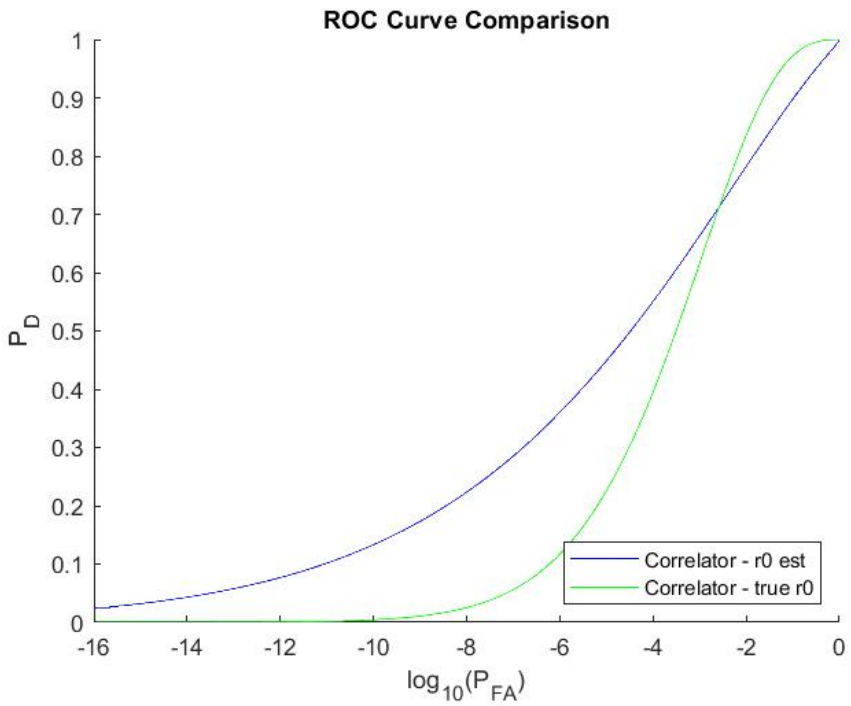

Figure 13: Matched Filter Performance (Day Conditions, SNR=1, r_0=2.5cm)

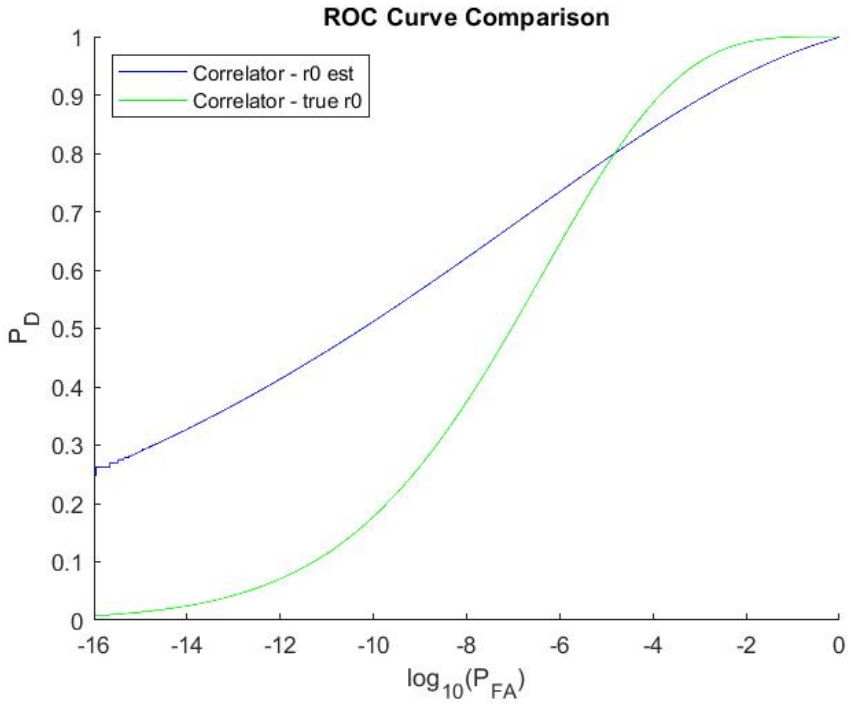

Figure 14**: Matched Filter Performance (Day Conditions, SNR=1.5, r_0=2.5cm)**

4. Short Exposure Frame Selector With r_0 Estimation

4.1 Chapter Overview

The other goal of this research was to test whether or not r_0 estimation could be implemented within a short exposure frame selector algorithm, and if so, what effect would it have. This section will explore how r_0 estimation was added to an existing short exposure frame selection algorithm that is based on research done by Connor Paw in his Master's Thesis [13]. This section will also cover the different simulated data sets that this algorithm was tested on, the different performance data collected on the algorithm, and the results of the simulations, to include detector performance and r_0 estimation accuracy.

Another topic that will be covered in this section is the comparison between the matched filter and frame selector algorithms. Both algorithms will be run using the same sets of data in order to compare their performance. ROC curves will be shown in order to visualize the difference in performance between the two algorithms, as well as how much r_0 estimation affects the performance of each algorithm.

4.2 Short Exposure Frame Selection Algorithm

The Frame Selection Algorithm used in this research is the same one that was described in section 2.8. It works by first finding the average SNR with all 10 frames summed together. Then it removes one frame at a time and recalculates the average SNR, repeating this process until the SNR has been recalculated once with each frame missing from the dataset, as shown in Equation 30 in section 2.8. Then it can rank the frames based on how much their removal from the dataset either increased or decreased the

SNR. Finally, it throws out the bad frames by removing the worst remaining frame and recalculating the SNR and then repeating this process until removing the worst frame no longer increases the average SNR by a significant amount. Then the remaining good frames get passed to the detection algorithm.

As was the case with the matched filter, the r_0 estimation is done before the detection code is run. The process for this estimation is the same one that was explained in section 3.5. It works by first generating 50 PSF's using 50 different r_0 values ranging between 0-5cm. Then, each of those PSFs are correlated with the simulated long exposure image for that given trial. The r_0 used to generate the PSF that best matches the data is used as the estimated r_0 for that trial. The estimated r_0 value is then fed to both detectors, ensuring that both detection algorithms are using the same data so that their performance can be compared accurately.

4.2.1 Bimodal Gaussian Model

One distinction between the traditional frame selection algorithm and the one used in this research is the assumption used to generate the ROC curves associated with the frame selector. One of the improvements that Paw made to the frame selector algorithm in his research was realizing that the traditional Gaussian assumption did not fit the data being produced by the frame selector, as shown in Figure 15. He found that a bimodal Gaussian model was more accurate, and therefore that is what should be used in order to generate the ROC curves for the frame selector data [13]. The equations for the new P_d and P_{fa} calculations under this bimodal Gaussian model are shown in Equations 32 and 33. These equations are each summations of two different Gaussian distributions

with different means and variances. The P_d equation uses the data from the H_1 case and the P_{fa} equation uses data from the H_0 case. In the equations, N_1 and N_2 are the number of frames that utilized either the frame selected value or the original summed frames correlator value, respectively. In these equations, $\sigma_{\Lambda_1}^2$ and $\sigma_{\Lambda_2}^2$ represent the variance of the LRT outputs from the first and second distribution, respectively, while μ_{Λ_1} and μ_{Λ_2} represent the means.

$$P_D = \frac{N_1}{N_1 + N_2} \int_{\tau}^{\infty} \frac{e^{\frac{-(\Lambda - \mu_{\Lambda_1})^2}{2\sigma_{\Lambda_1}^2}}}{\sqrt{2\pi}\sigma_{\Lambda_1}^2} d\Lambda + \frac{N_2}{N_1 + N_2} \int_{\tau}^{\infty} \frac{e^{\frac{-(\Lambda - \mu_{\Lambda_2})^2}{2\sigma_{\Lambda_2}^2}}}{\sqrt{2\pi}\sigma_{\Lambda_2}^2} d\Lambda \tag{32}$$

$$P_{FA} = \frac{N_1}{N_1 + N_2} \int_{\tau}^{\infty} \frac{e^{\frac{-(\Lambda - \mu_{\Lambda_1})^2}{2\sigma_{\Lambda_1}^2}}}{\sqrt{2\pi}\sigma_{\Lambda_1}^2} d\Lambda + \frac{N_2}{N_1 + N_2} \int_{\tau}^{\infty} \frac{e^{\frac{-(\Lambda - \mu_{\Lambda_2})^2}{2\sigma_{\Lambda_2}^2}}}{\sqrt{2\pi}\sigma_{\Lambda_2}^2} d\Lambda \tag{33}$$

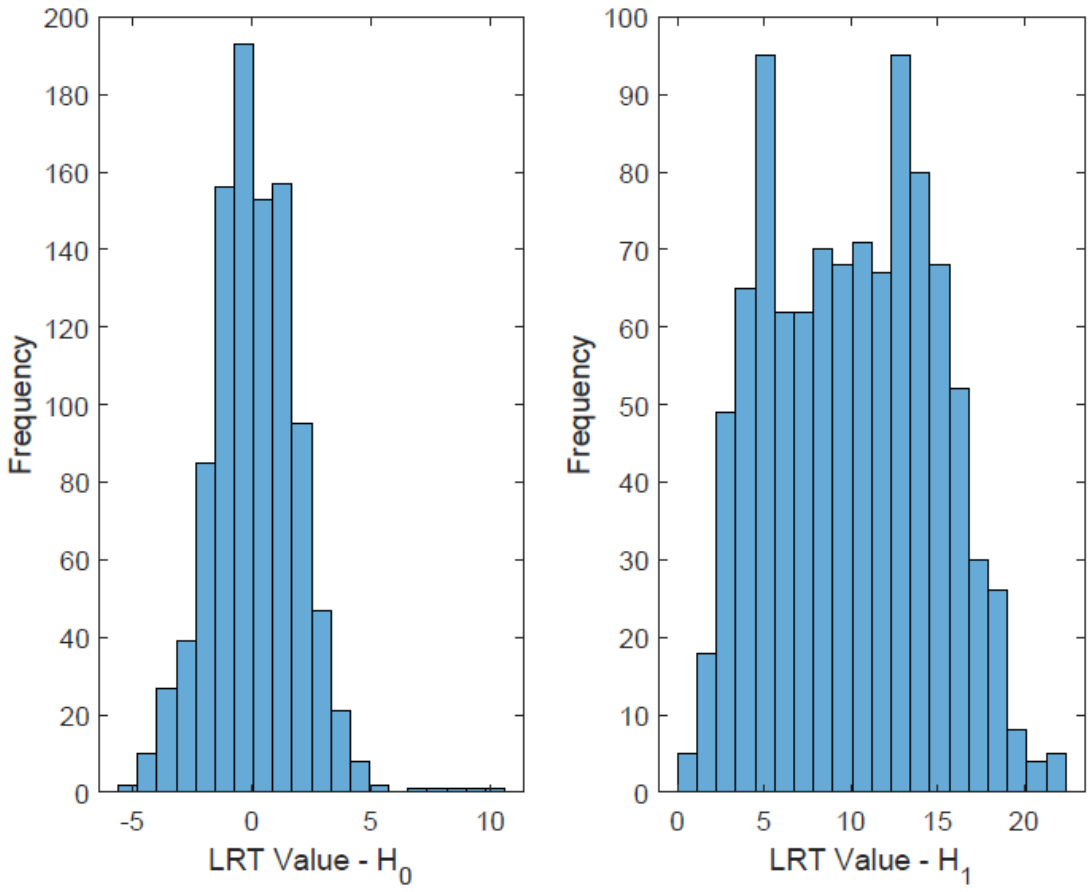

Figure 15: Histograms of LRT Values for H_0 and H_1

4.3 Simulated Data

Since both detection algorithms are using the same data, the parameters used to generate the sample datasets are the same as in the previous chapter. Table 1 in section 3.4 shows all of the parameters used to generate the sample data, including the variables that were changed to represent different conditions and the levels of those variables that were tested.

To generate the simulated short exposure data, we had to be able to accurately model a short exposure OTF, which meant needing to use a unique set of Zernike

polynomials at each individual time instance corresponding to a short exposure image being taken (approximately every 10ms). To do this, we relied on past research done by AFIT student Isaac Putnam [15]. For his research, he wrote code that was able to produce many individual Zernike phase screens that are all correlated in time. Our research leverages his findings in order to create our time-correlated short exposure data, which is then given to the detection algorithms. Without having these temporally correlated phase screens to accurately generate our short exposure PSFs, our data would not be true simulated short exposure data.

Example PSFs of objects generated by the code are shown below in Figures 16 and 17. Figure 16 shows an example short exposure image of a bright space object (SNR=1.5) with no noise present in the image. Figure 17 shows an image of the same object with background and photon counting noise present. As shown in the figures, even a bright object becomes indistinguishable to the naked eye when looked at against a noisy background. This is part of the challenge posed to the detection algorithms, being able to pick out these objects that seemingly blend in with the background. Figure 18 also shows a series of short exposure frames without noise displayed in quick succession. This is a good visualization of the jitter that was discussed in section 2.3.4. It shows the object moving around from frame to frame, as well as appearing to change shape in some frames. This movement of the object is what is averaged out in the simulated long exposure image shown in the last chapter.

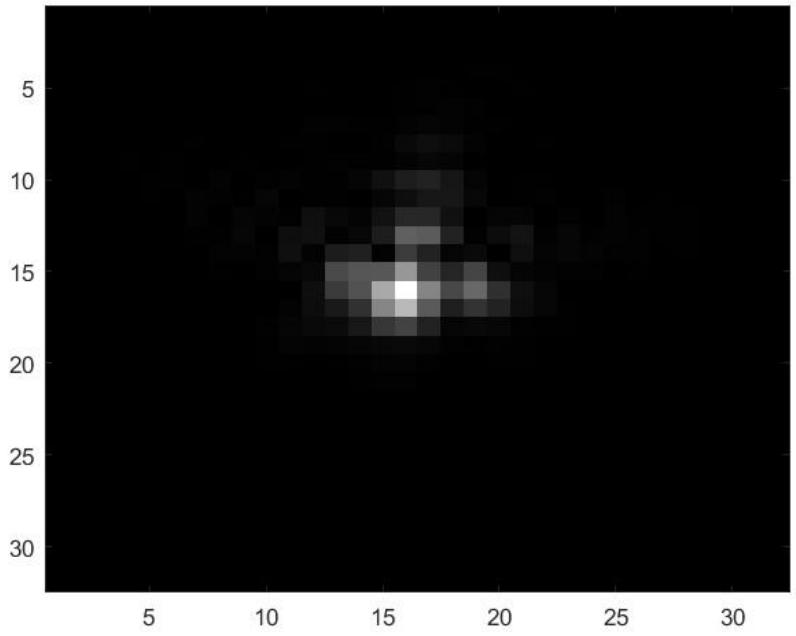

Figure 16: Short Exposure Point Source Image With no Noise

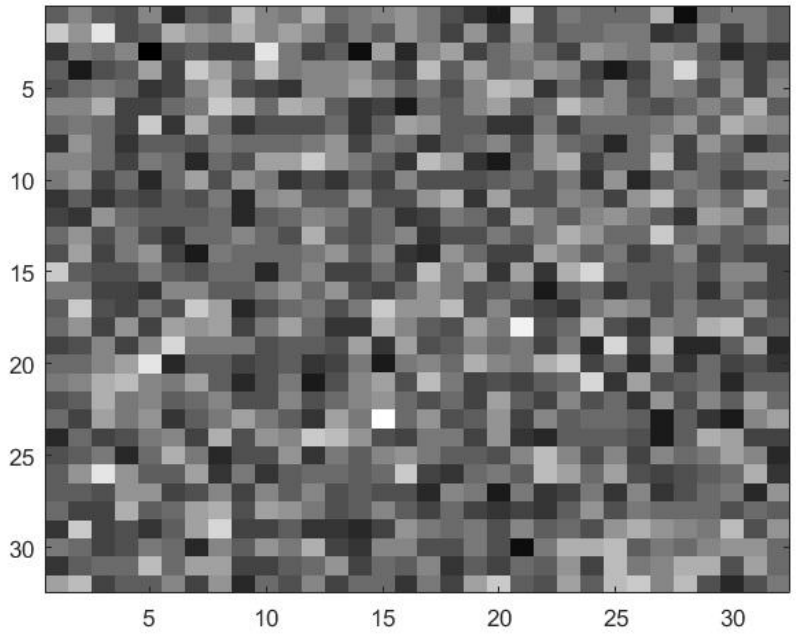

Figure 17: Short Exposure Point Source Image With Noise

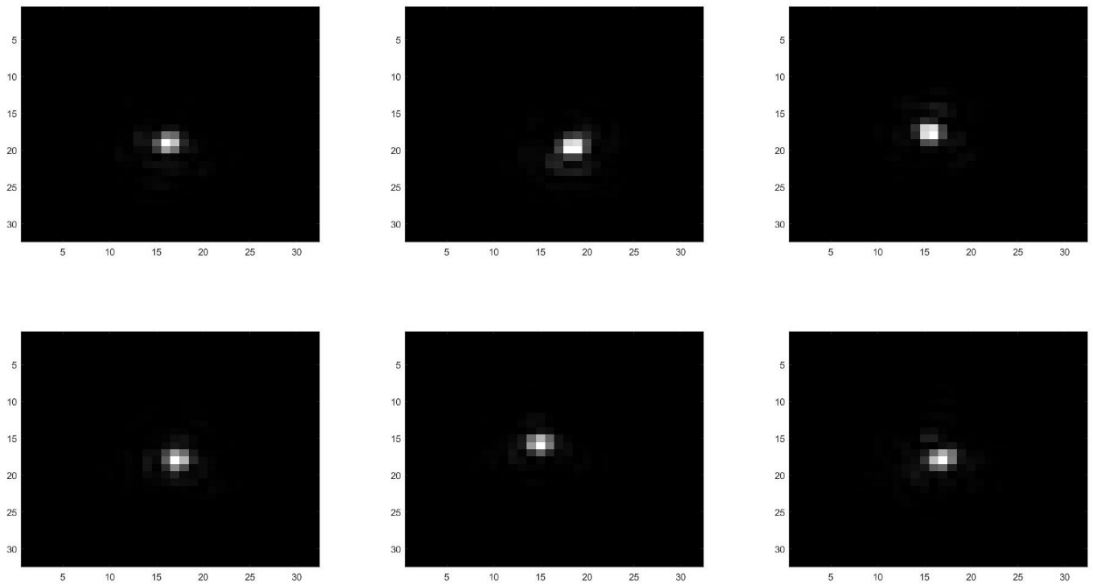

Figure 18: Series of Consecutive Short Exposure Frames

4.4 Frame Selector Results

The main thing being tested in this research is the impact that r_0 estimation has on the short exposure frame selection algorithm and whether or not the algorithm is able to maintain its detection performance when using r_0 estimation as opposed to just knowing the true r_0 value. To test this, similarly to the matched filter case, the frame selector code was run twice on the same dataset, once using r_0 estimation and once when being provided the true r_0 value. There were then 2 ROC curves generated, allowing us to compare the performance of the algorithm on the same dataset, with the only thing changing being the method they use to get their r_0 value. As with Chapter 3, for each variable, there were 3 ROC curves generates, one for each level of said variable, in order

to judge the impact each variable had on the detection algorithms and to see if that variable affected one algorithm more than another.

4.4.1 Frame Selector Comparison – Time of Day

As with the matched filter algorithm, the frame selector actually showed improved detection performance over most of the range of P_{fa} values when the time of day (background brightness) was varied. The frame selector improved by a much smaller margin than the matched filter, only increasing P_d by an average of 5% at a P_{fa} of 10^{-9}, but like the matched filter, it improved in every scenario that was tested. Figures 19-21 show the performance of the algorithm in all 3 lighting scenarios, with all the other variables remaining the same.

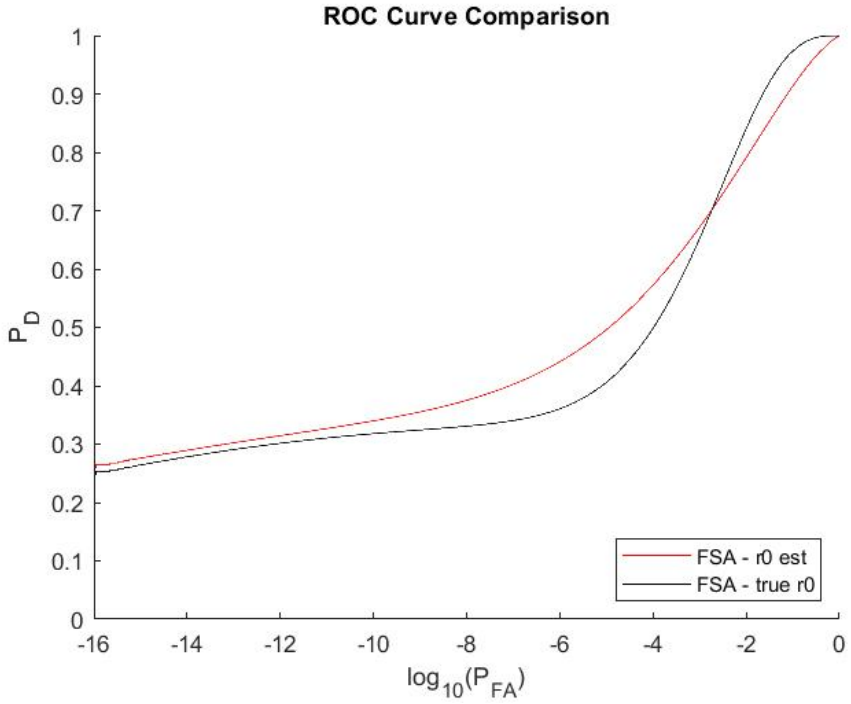

Figure 19: Frame Selector Performance (Day Conditions, SNR=1, r_0=2.5cm)

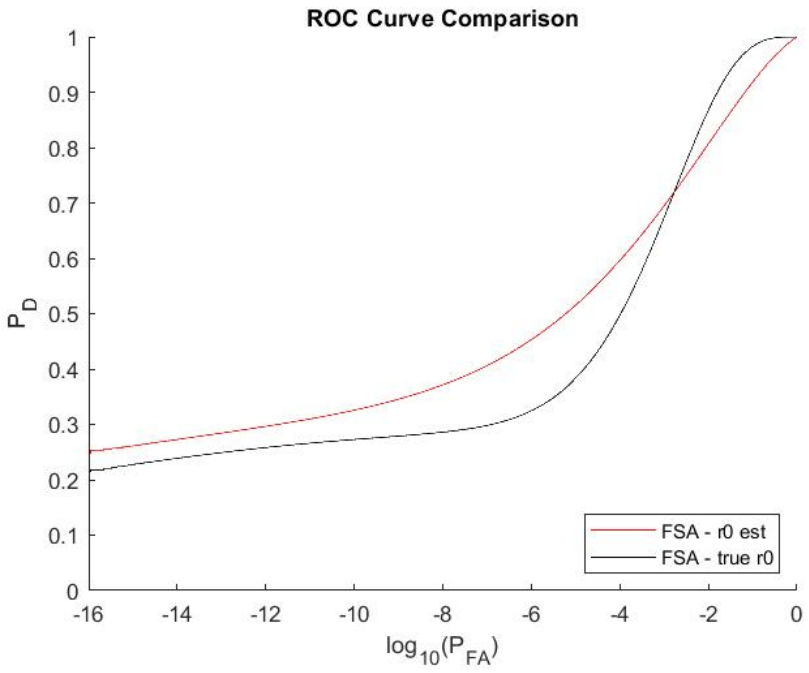

Figure 20: Frame Selector Performance (Night Conditions, SNR=1, r_0=2.5cm)

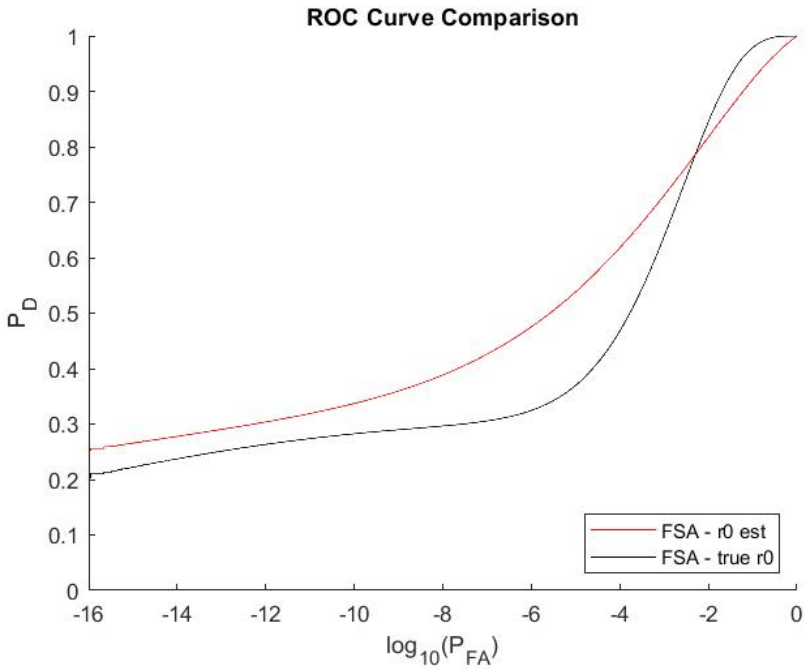

Figure 21: Frame Selector Performance (Dusk/Dawn Conditions, SNR=1, r_0 =2.5cm)

4.4.2 Frame Selector Comparison – Changes in True r_0

Similarly to the matched filter, changes in the true r_0 value have a large effect on the performance of the frame selector. Also similarly to the matched filter, the frame selector using the true r_0 slightly outperforms the one using r_0 estimation, although both of them have extremely low P_d values at P_{fa}=10^{-9}. As r_0 increases, the frame selector using r_0 estimation overtakes the one without in performance, and at higher r_0 values that performance gap grows, reaching 26% at r_0=4cm.

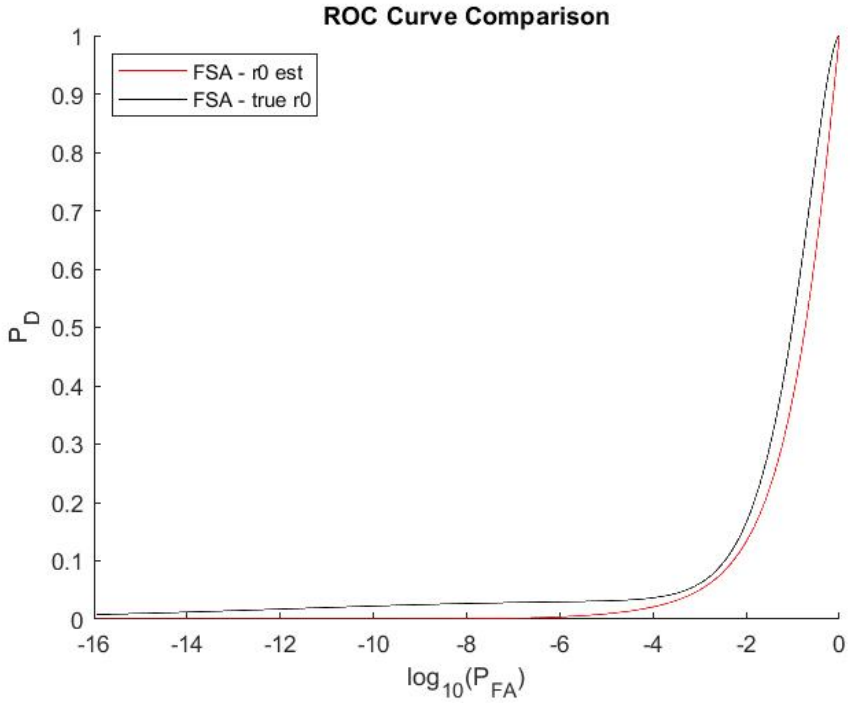

Figure 22: Frame Selector Performance (Day Conditions, SNR=1, r_0=1cm)

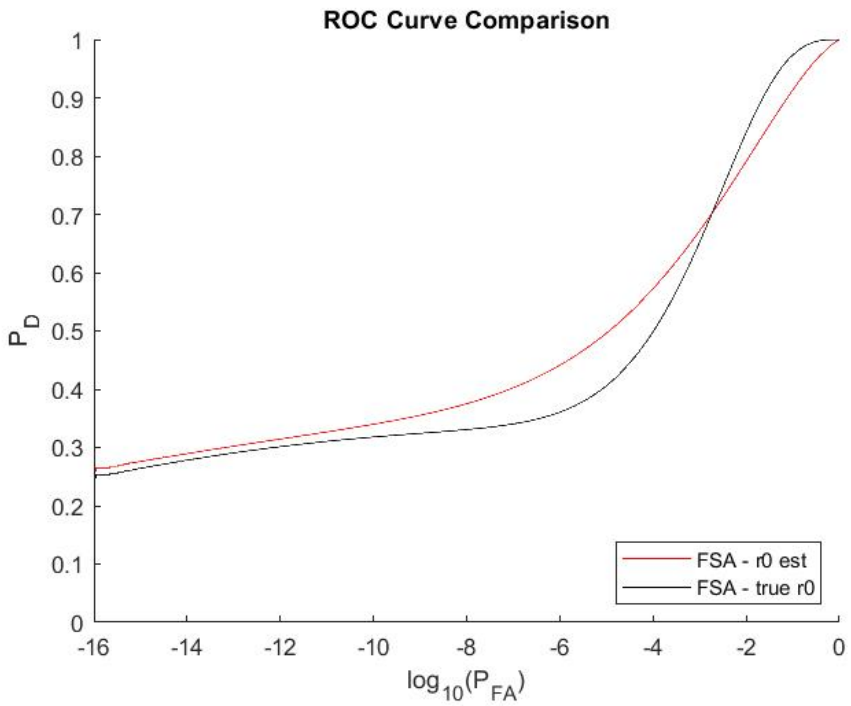

Figure 23: Frame Selector Performance (Day Conditions, SNR=1, r_0=2.5cm)

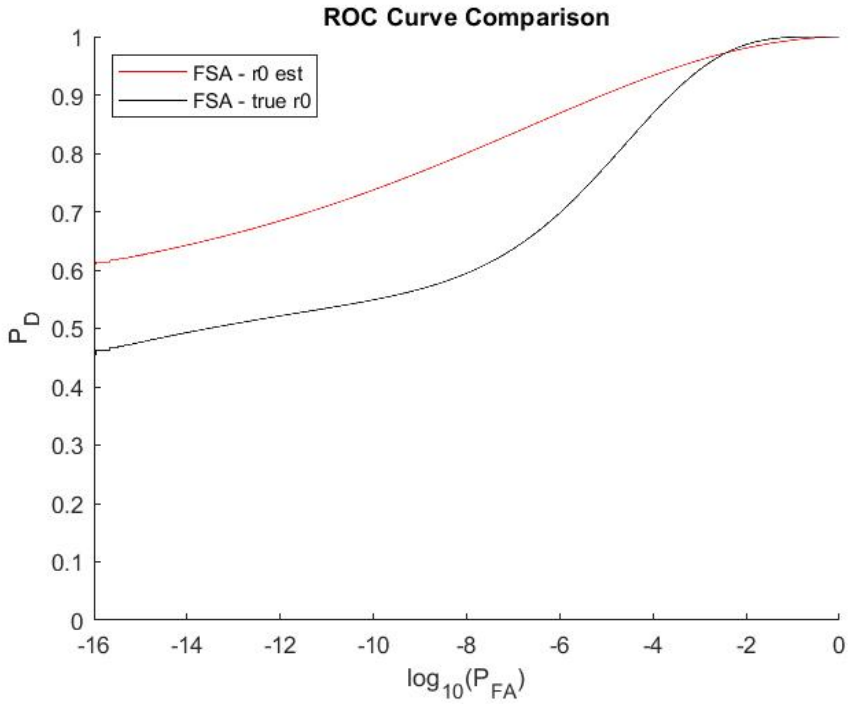

Figure 24: Frame Selector Performance (Day Conditions, SNR=1, r_0=4cm)

4.4.3 Frame Selector Comparison – Object Brightness

The last variable to test for the frame selector is object brightness. As shown in Figures 25-27, the brightness of the object being detected does have a fairly significant effect on the performance of the detection algorithms. Also, at every brightness level, the frame selector with r_0 estimation outperforms the one without, albeit by a slim margin. Another noteworthy observation is that increases in object brightness do not lead to a significant increase in the performance gap between the two algorithms, as in the case with the changes in true r_0 value discussed in the previous section. There is a slight increase in the performance gap at SNR=1.5, with the change in performance between the algorithms growing to 10% at P_{fa}=10^{-9}, but this is not as significant an increase as we see with changes in r_0.

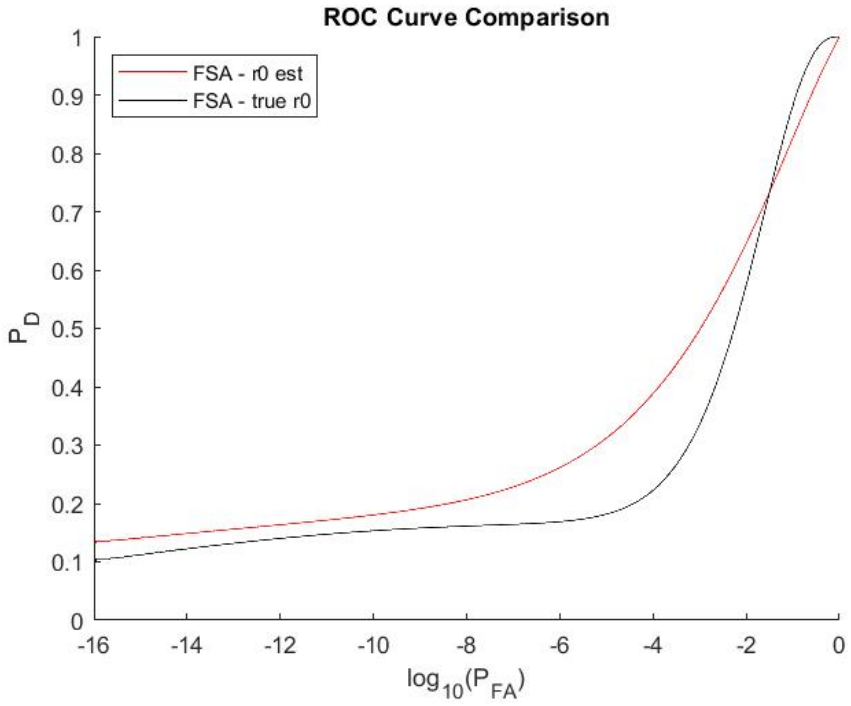

Figure 25**: Frame Selector Performance (Day Conditions, SNR=0.75, r_0=2.5cm)**

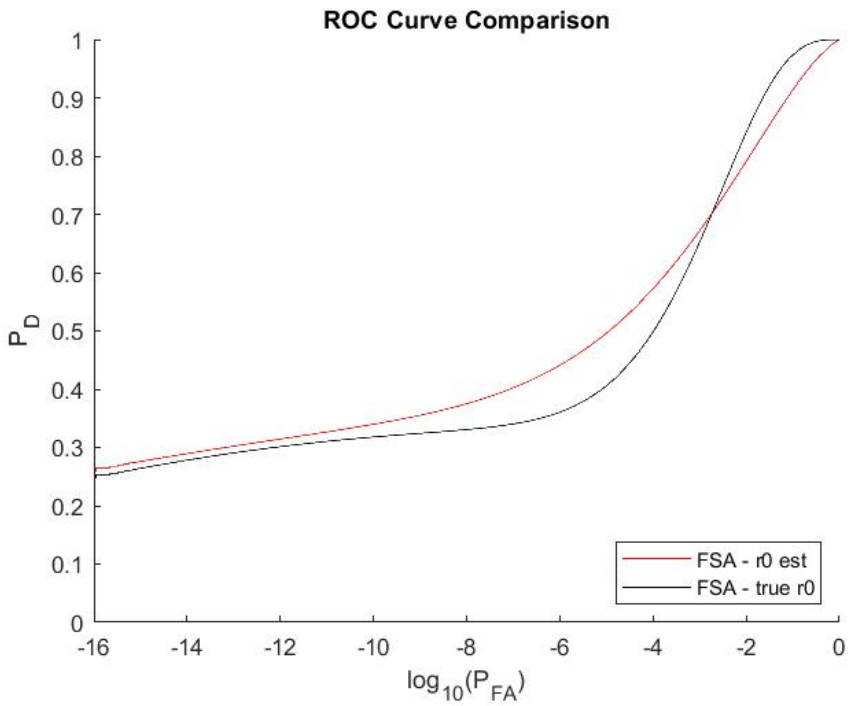

Figure 26: Frame Selector Performance (Day Conditions, SNR=1, r_0=2.5cm)

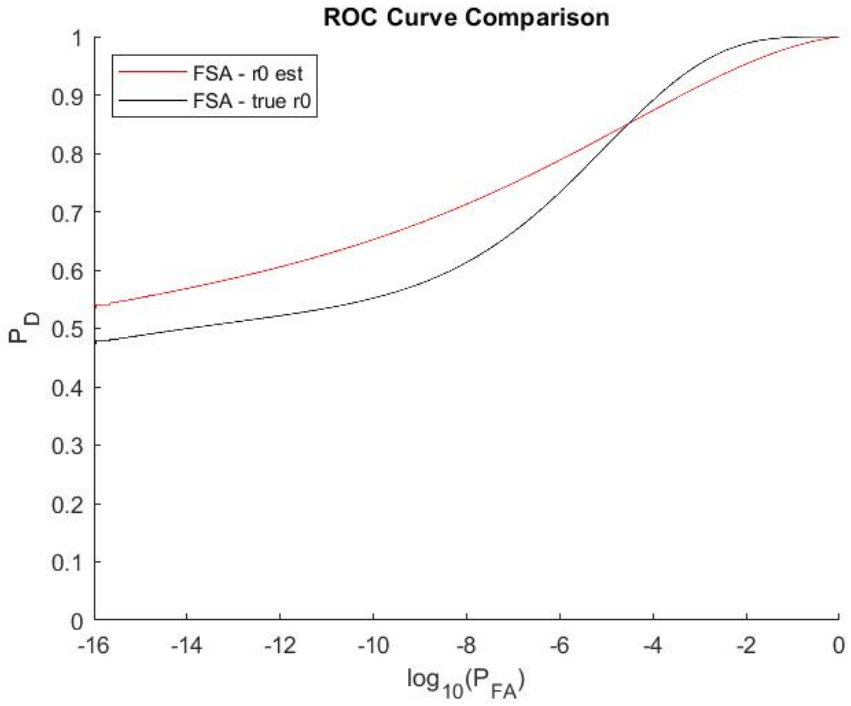

Figure 27: Frame Selector Performance (Day Conditions, SNR=1.5, r_0=2.5cm)

4.5 Frame Selector vs. Matched Filter

The final comparison to be made was the difference in performance between the matched filter and frame selector. This was done by combining the ROC curves from Chapters 3 and 4 in order to visualize all four detection algorithms' performance under the same sets of conditions. This allows us to visualize which algorithms perform best, which ones are most affected by changes in our variables, and what the gap in performance between the different algorithms is.

As shown in Figures 28-36, in eight of the nine scenarios we tested, the frame selector using r_0 estimation performed the best at our target P_{fa} of 10^{-9}. The one exception to this was when we tested a low r_0 value of 1 cm. In that scenario, the frame selector without r_0 estimation outperformed all the other detectors, although all four of them had a P_d below 5% over almost the entire range of P_{fa} values. In most of the conditions, the frame selector without r_0 estimation performed the second best, although there were some sets of conditions where the matched filter with r_0 estimation was either at a similar performance level or actually outperformed it. The scenarios where this happened tended to be when the conditions were better for imaging, such as r_0 being high, SNR being high, or nighttime imaging. In scenarios where the imaging conditions were less ideal, the frame selector outperformed the matched filter by a more significant margin.

4.5.1 Frame Selector vs. Matched Filter – Time of Day

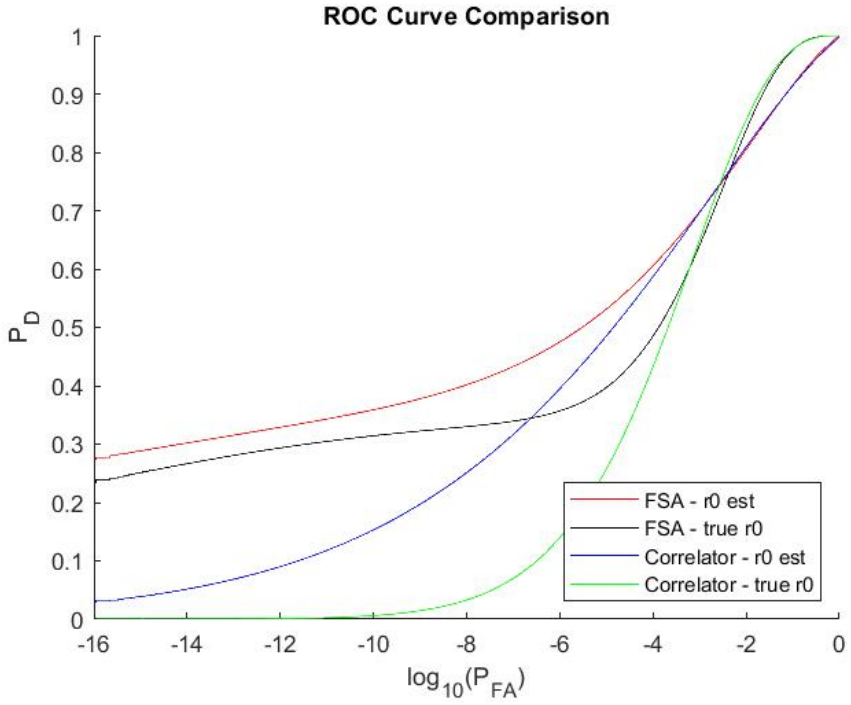

Figure 28: All Detectors Performance (Day Conditions, SNR=1, r_0=2.5cm)

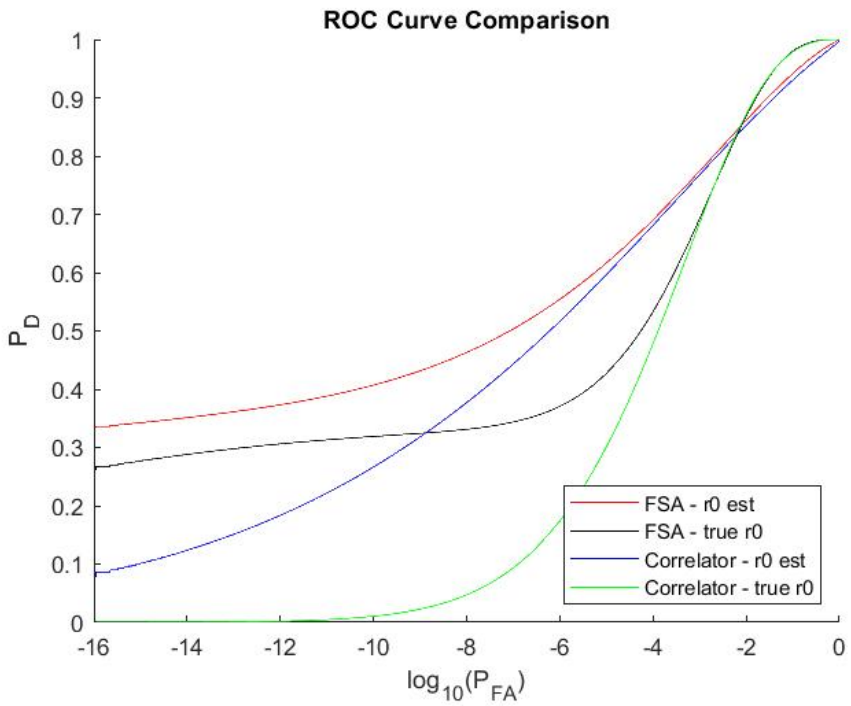

Figure 29: All Detectors Performance (Dusk/Dawn Conditions, SNR=1, r_0=2.5cm)

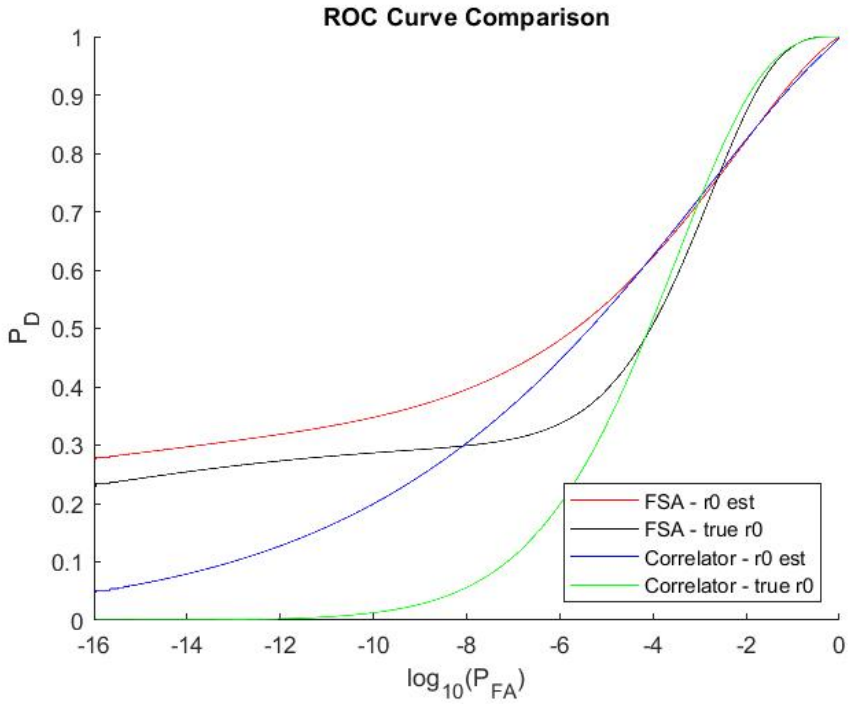

Figure 30: All Detectors Performance (Night Conditions, SNR=1, r_0=2.5cm)

4.5.2 Frame Selector vs. Matched Filter – Changes in True r_0

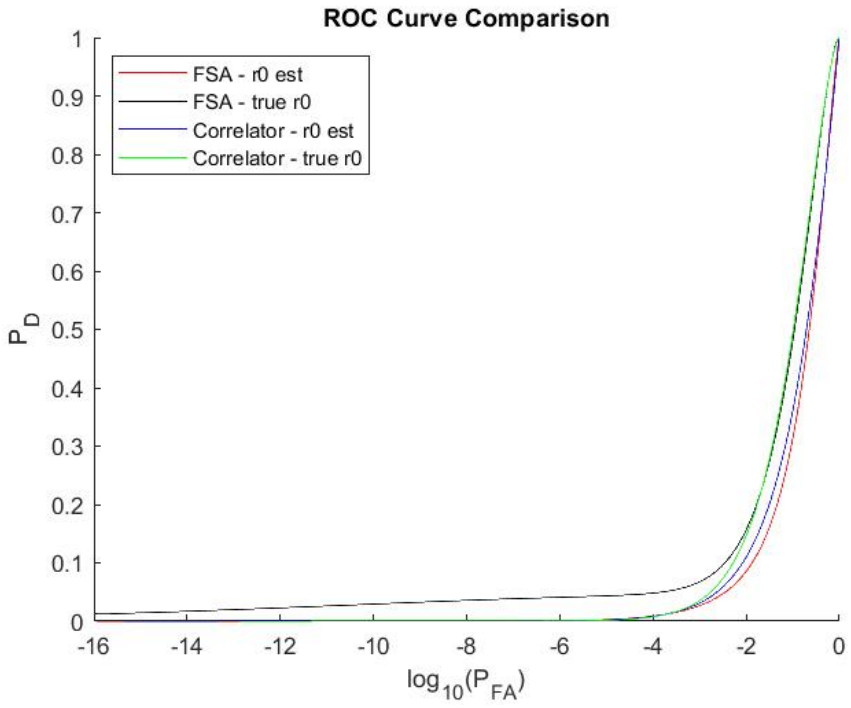

Figure 31: All Detectors Performance (Day Conditions, SNR=1, r_0=1cm)

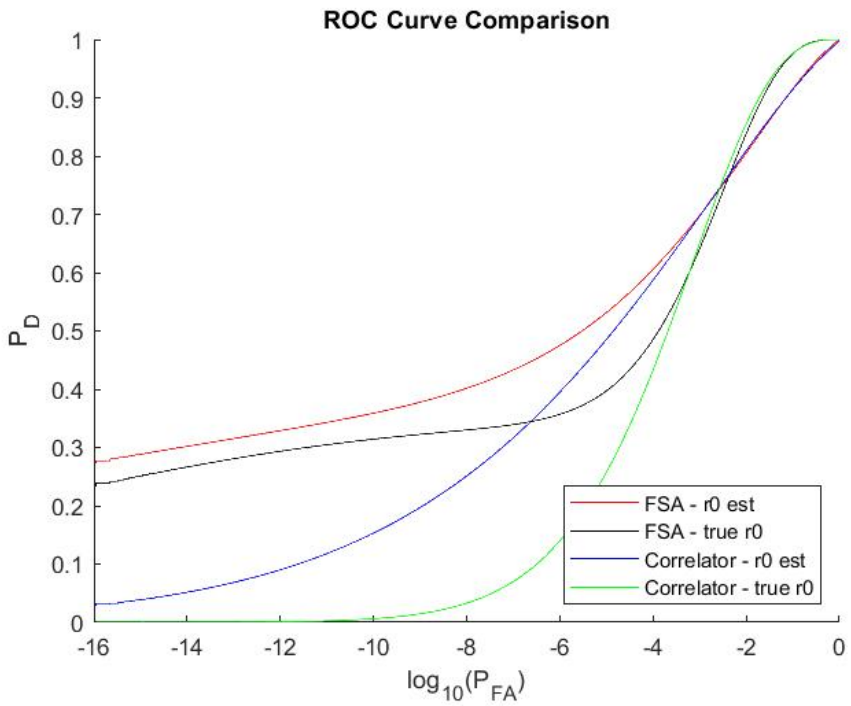

Figure 32: All Detectors Performance (Day Conditions, SNR=1, r_0=2.5cm)

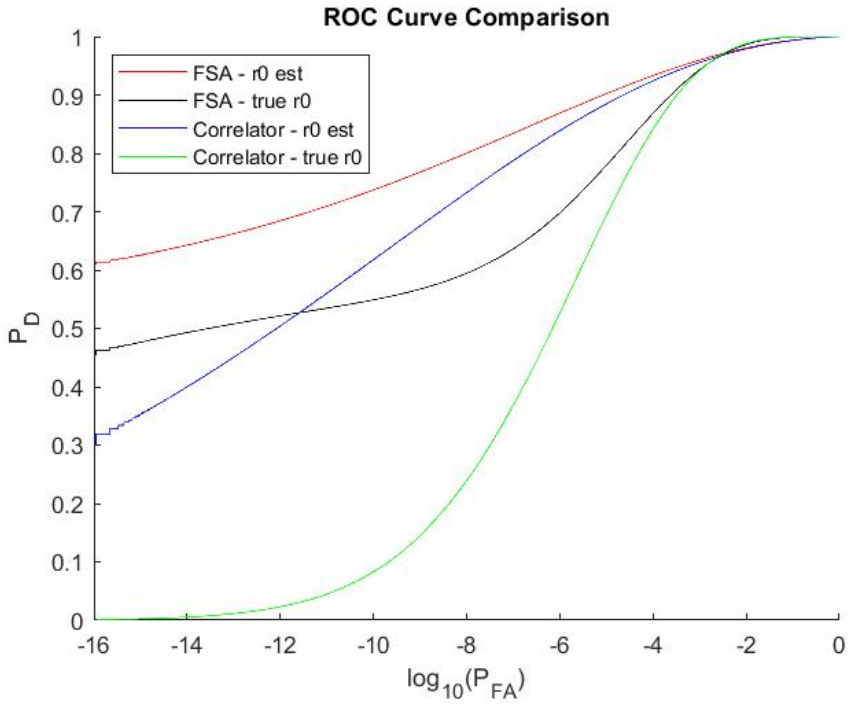

Figure 33: All Detectors Performance (Day Conditions, SNR=1, r_0=4cm)

4.5.3 Frame Selector vs. Matched Filter – Object Brightness

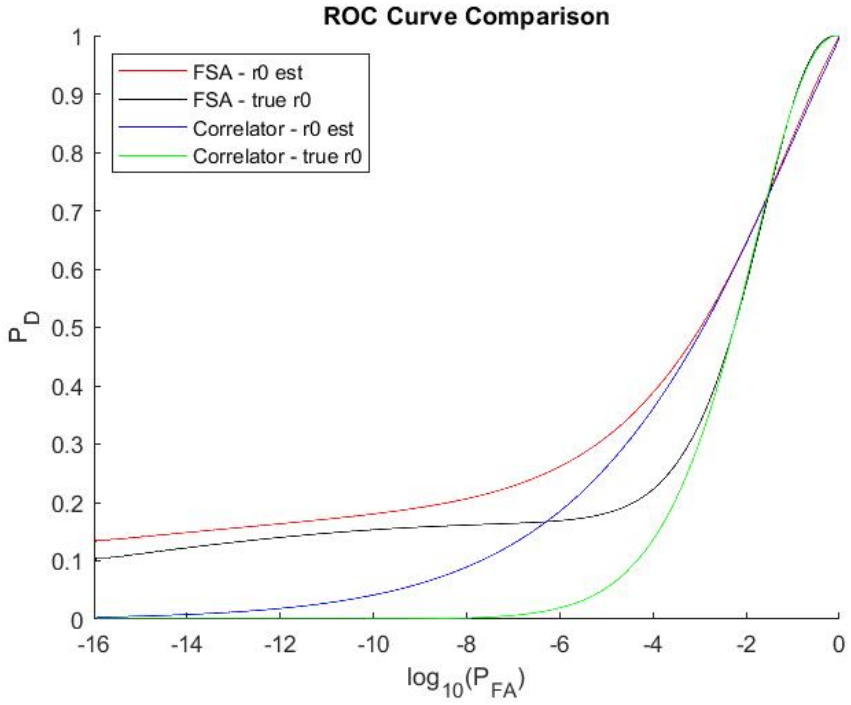

Figure 34: All Detectors Performance (Day Conditions, SNR=0.75, r_0=2.5cm)

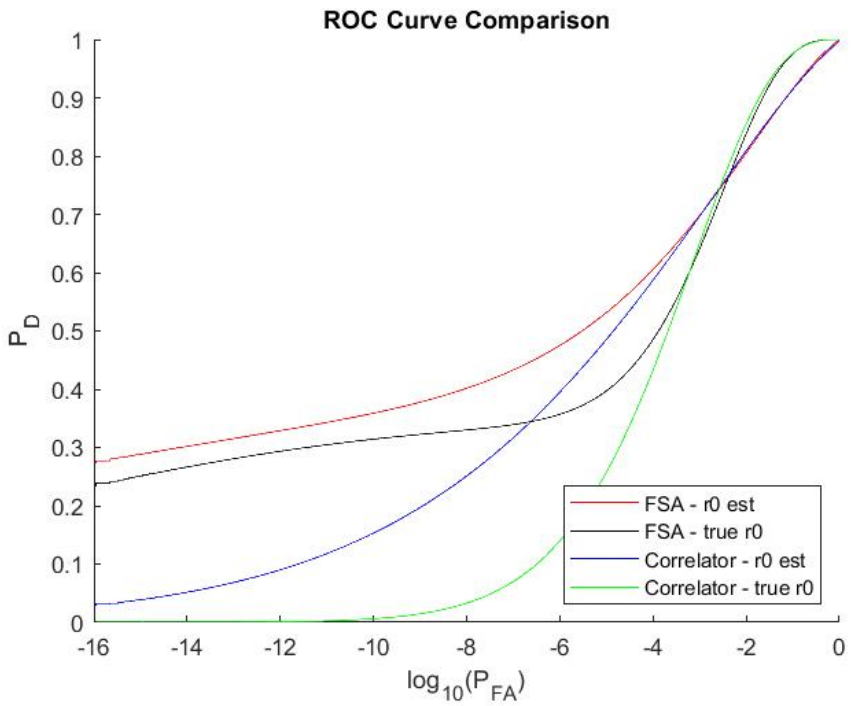

Figure 35: All Detectors Performance (Day Conditions, SNR=1, r_0=2.5cm)

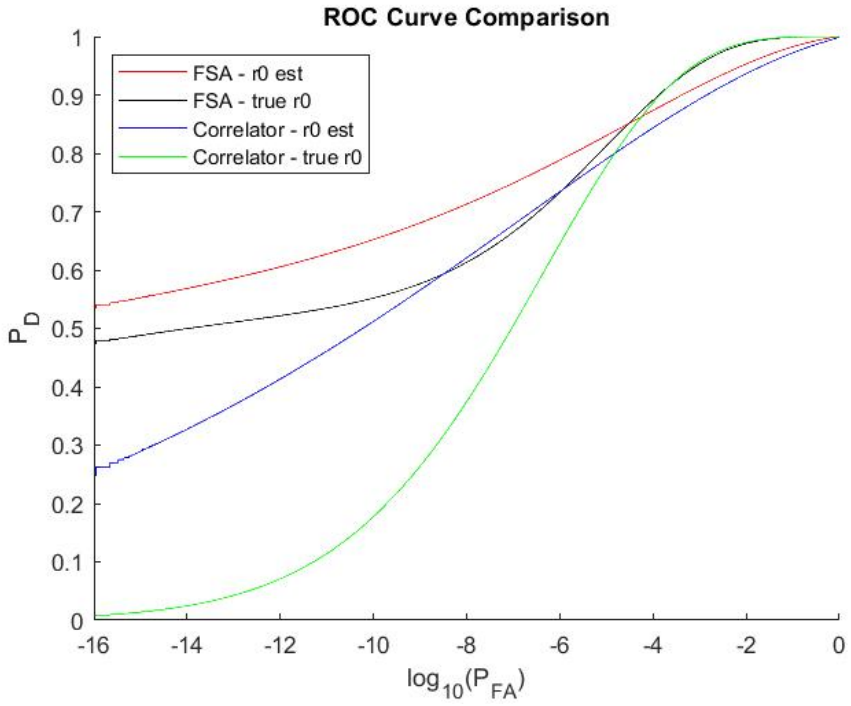

Figure 36: All Detectors Performance (Day Conditions, SNR=1.5, r_0=2.5cm)

5. Conclusion

5.1 Chapter Overview

This chapter will sum up the results that were achieved in Chapters 3 and 4, drawing conclusions about the effect r_0 estimation had on each algorithm, as well as the comparison between the performance of the two algorithms. It will also discuss ongoing challenges to this research, the significance of this research to the DoD as well as the space community as a whole, and opportunities for future work and improvements to the algorithms.

5.2 Research Conclusions

The main goal of this research was to successfully implement a r_0 estimation component within the existing structure of the short exposure matched filter and frame selector detection algorithms. This research sought to prove that these detection algorithms could achieve similar detection performance while having less information available to them. What happened during the simulation was that implementing r_0 estimation actually improved the performance of both detectors in almost all of the conditions we tested. The matched filter performance was improved significantly when using r_0 estimation, while the short exposure frame selection algorithm was also improved, but generally by a smaller margin. Both algorithms showed improvement across almost the entire range of conditions that were tested in this research, showing that this improvement was not just a specific phenomenon that only happened over a narrow range of conditions.

The improvement in performance shown by both algorithms is something that was initially unexpected at the beginning of this research because it is something unique to the short exposure case. In any long exposure applications, adding r_0 estimation will decrease the performance of the detector by at least a small margin, however, due to fluctuations in the image r_0 in the short exposure case, r_0 estimation actually led to increased detector performance.

Another takeaway from this research is that, the short exposure frame selector provided the best overall detector performance when using r_0 estimation. Even without r_0 estimation, it often outperformed the matched filter both with and without r_0 estimation. This is because the frame selector algorithm is designed for short exposure imagery applications, whereas the matched filter is designed primarily for long exposure imagery and had been modified to process short exposure imagery for this research. However, even despite the drawbacks facing the matched filter algorithm, adding r_0 estimation improved its performance significantly, to the point where it was competitive with the frame selector that wasn't using r_0 estimation in many of the cases that were tested, and even outperformed it in some scenarios. This is significant because it means that when r_0 estimation is added, it takes the matched filter from an algorithm that is practically unusable for short exposure applications to one that can be used under certain conditions to provide performance that rivals the traditional frame selector without r_0 estimation.

5.3 Significance of Research

Space object detection is an area that will only continue to increase in importance as the number of space objects continues to increase. This means that evolutions and

improvements to the technology and algorithms that are used in space object detection are both necessary and important. What makes this research, as well as the research prior to it that it is based on, important is the fact that they introduce possible improvements to the algorithms that are currently being used for these applications. This research provides a proof of concept that r_0 estimation can not only maintain, but actually improve detector performance in the short exposure case, and that the matched filter becomes a viable short exposure detection algorithm when r_0 estimation is used.

5.4 Recommendations for Future Research

There are several ways to continue and improve upon the research done in this paper. The first one would be to test the algorithms on real world data as opposed to just simulated data sets. Conformation that the algorithms provide roughly the same performance on real and simulated data would be one step closer to implementing this research in detectors for real world applications.

Another possible improvement would be to test the algorithm under a wider range of conditions. Expanding the range of r_0 values, testing a larger number of object brightness's and lighting values, and even varying the telescope parameters would all provide a more complete picture of how the algorithms perform under varying conditions.

A final recommendation for future work would be to add confidence intervals to the ROC curves to determine with a level of certainty how different the results are from each other. This would add more context and certainty to the results that were observed in this research.

Bibliography

1. J. Garamone, “Chief of Space Operations Discusses Need for Outreach to Partners, State of Space Force”, *Defense.gov*, 25 November 2020, Retrieved 2 June 2021, https://www.defense.gov/Explore/News/Article/Article/2427918/
2. National Aeronautics and Space Administration, “Space Debris and Human Spacecraft”, 26 May 2021, Retrieved 2 June 2021, https://www.nasa.gov/mission_pages/station/news/orbital_debris.html
3. National Aeronautics and Space Administration, “Debris Remediation”, Retrieved 2 June 2021, https://www.orbitaldebris.jsc.nasa.gov/remediation/
4. Joint Chiefs of Staff (JCS), JP 3-14, *Space Operations*., 26 October 2020, Retrieved 3 June 2021, https://www.jcs.mil/Portals/36/Documents/Doctrine/pubs/jp3_14ch1.pdf?ver=-zw88OCRWcvI913jycR-uQ%3D%3D
5. J. W. Goodman, *Statistical Optics, 2nd ed*, pp 419-435, John Wiley & Sons, Inc., 2015.
6. D. J. Becker, “Techniques for Improved Space Object Detection Performance from Ground-Based Telescope Systems Using Long and Short Exposure Images,” *Def. Tech. Inf. Cent.*, 2018.
7. J. W. Goodman, “Introduction to Fourier Optics, 3rd Edition,” *Roberts & Company Publishers*. 2005.
8. J. W. Goodman, *Statistical Optics, 2nd ed*, pp 366-368, John Wiley & Sons, Inc., 2015.
9. C. Max, “Introduction to Adaptive Optics and Its History”, *American Astronomical Society 197th Meeting*
10. J. C. Zingarelli, “Enhancing Ground Based Telescope Performance with Image Processing,” *Def. Tech. Inf. Cent*., 2013.
11. H. E. M. Viggh, G. H. Stokes, F. C. Shelly, M. S. Blythe, and J. S. Stuart, “Applying electro-optical space surveillance technology to asteroid search and detection: The LINEAR program results,” in *Space 1998*, 1998, doi: 10.1061/40339(206)44.
12. S. C. Pohlig, “An Algorithm for Detection of Moving Optical Targets,” *IEEE Trans. Aerosp. Electron. Syst.*, 1989, doi: 10.1109/7.18661.
13. C. Paw, “Supporting Space Domain Awareness Through the Development and Analysis of Space Object Detection Algorithms Employed by Ground-Based Telescopes,” Air Force Institute of Technology, 2021
14. G. Graupmann, “Enhanced Space Object Detection Without Prior Knowledge of the Point Spread Function,” Air Force Institute of Technology, 2021
15. I. B. Putnam, “Atmospheric Impact on Long Pulse Laser Detection and Ranging (LADAR) Systems,” Air Force Institute of Technology, 2013.

REPORT DOCUMENTATION PAGE

Form Approved
OMB No. 0704-0188

1. REPORT DATE *(DD-MM-YYYY)*	2. REPORT TYPE	3. DATES COVERED *(From - To)*
03/24/2022	Master's Thesis	Sept 2020 - March 2022

4. TITLE AND SUBTITLE

Estimating Atmospheric Turbulence Within a Short Exposure Frame Selection Algorithm

5a. CONTRACT NUMBER

5b. GRANT NUMBER

5c. PROGRAM ELEMENT NUMBER

6. AUTHOR(S)

DeLuca, Aaron, 1st Lt, USAF

5d. PROJECT NUMBER

5e. TASK NUMBER

5f. WORK UNIT NUMBER

7. PERFORMING ORGANIZATION NAME(S) AND ADDRESS(ES)
Air Force Institute of Technology
Graduate School of Engineering and Management (AFIT/EN)
2950 Hobson Way
Wright-Patterson AFB OH 45433-7765

8. PERFORMING ORGANIZATION REPORT NUMBER

AFIT-ENG-MS-22-M-022

9. SPONSORING/MONITORING AGENCY NAME(S) AND ADDRESS(ES)

Intentionally Left Blank

10. SPONSOR/MONITOR'S ACRONYM(S)

11. SPONSOR/MONITOR'S REPORT NUMBER(S)

12. DISTRIBUTION/AVAILABILITY STATEMENT

DISTRIBUTION STATEMENT A:
APPROVED FOR PUBLIC RELEASE; DISTRIBUTION UNLIMITED.

13. SUPPLEMENTARY NOTES

14. ABSTRACT

Space is becoming an increasingly crowded domain. As it becomes more congested, the ability to accurately detect and track objects, both natural and man-made, becomes more and more important. Having an accurate space surveillance network allows us to protect our own space assets while also maintaining awareness of foreign space assets and threats to our satellites such as debris and small meteorites. This means that the ability to detect small, dim objects is key to being able to protect our space assets. This thesis will seek to expand on and improve certain existing space object detection techniques and algorithms.

15. SUBJECT TERMS

Space object detection, atmospheric turbulence, daylight imaging, image processing, short exposure

16. SECURITY CLASSIFICATION OF:			17. LIMITATION OF ABSTRACT	18. NUMBER OF PAGES	19a. NAME OF RESPONSIBLE PERSON
a. REPORT	b. ABSTRACT	c. THIS PAGE			Maj David J. Becker, AFIT/ENG
					19b. TELEPHONE NUMBER *(Include area code)*
U	U	U	UU	76	937-255-3636 x4371 david.becker@afit.edu